Marine and Petroleum Geology 181 (2025) 107513

Contents lists available at ScienceDirect

Marine and Petroleum Geology

journal homepage: www.elsevier.com/locate/marpetgeo

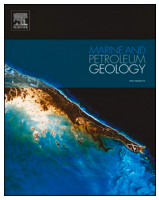

Thermal records of carbonate cements: Deciphering the hydrothermal imprint on Eocene Shahejie Formation sandstones in the northern Dongying Depression, China

Yishan Gao [a,b], Shifa Zhu [a,b,*], Hang Cui [a,b,**], Wendian Cai [a,b], Ruihang Zhang [a,b]

[a] National Key Laboratory of Petroleum Resources and Engineering, China University of Petroleum (Beijing), Beijing, 102249, China
[b] College of Geosciences, China University of Petroleum, Beijing, 102249, China

ARTICLE INFO

Keywords:
Carbonate cements
Material origins
Formation mechanisms
Hydrothermal activities
Shahejie formation
Dongying depression
U-Pb geochronology

ABSTRACT

The carbonate cements in the sandstones of the Eocene Shahejie Formation in the Dongying Depression record crucial temporal and thermal information related to hydrothermal activity. This study presents a comprehensive investigation of these carbonate cements, detailing their diagenetic process, chronological formation, and material origins. Sedimentological evidence indicates that the sandstones in the study area were predominantly deposited in deltaic and marginal lacustrine settings, with a subdivision into matrix-rich and matrix-poor types at the microscale. Petrographic observation and electron probe microanalysis (EPMA) reveal that calcite is the predominant authigenic mineral phase, exhibiting variability in both abundance and morphology depending on sandstones maturity. Matrix-poor sandstones, characterized by higher maturity, predominantly exhibit blocky calcite cement, whereas those with a rich matrix and lower maturity tend to develop scattered patchy calcite. Fluid inclusion homogenization temperatures indicate that these calcite cements precipitated under abnormally high-temperature conditions, ranging from 85 to 350 °C. And the carbonate cements exhibit low $\delta^{13}C$ (−11.8 to −3.1 ‰ VPDB) and $\delta^{18}O$ (clustered tightly from −14.0 to −11.1 ‰ VPDB) values, interpreted to reflect a mixed source comprising magmatic CO_2, air CO_2, and a potential contribution from soil CO_2. *In situ* U-Pb isotopic dating of calcite constrains the timing of carbonate cement precipitation, with ages ranging from 39.4 ± 1.9 Ma to 42 ± 7.6 Ma. Ultimately, the results indicate that the calcium source for the carbonate cements in the Eocene Shahejie Formation sandstones of this region is primarily a mixture of primary alkaline formation waters and hydrothermal fluids. The carbon source is dominated by a mixture of magmatic CO_2 and air CO_2, with a potential minor contribution from soil CO_2. This study suggests that the hydrothermal activity influencing carbonate cementation in the study area was likely associated with the Cenozoic subduction of the New Pacific Plate. Through the integration of multiple advanced analytical techniques, this study elucidates the material origins and precipitation timing of hydrothermal derived carbonate cements, validating the potential application of advanced techniques such as *in situ* U-Pb isotopic dating of calcite in clastic rock research. Additionally, the hydrothermal activity age determined for the Shahejie Formation in this study provides crucial data support for the research on tectonic-magmatic activity in the Dongying Depression.

1. Introduction

Hydrothermally derived carbonate cements are widely developed across multiple layers in various basins (Liang et al., 2024; Cui et al., 2024). However, the extent to which carbonate cements are influenced by hydrothermal fluids and the mechanisms by which these fluids drive cementation remain active areas of research. The dissolution and precipitation processes of carbonate cements are controlled by various factors, including temperature, pressure, and the chemical composition of the fluids (Carvalho et al., 1995; Morad, 1998; Worden and Burley, 2003; Morad et al., 2010; Xi et al., 2019; Luo et al., 2020). Generally, rapid temperature drop, low pressure, and high salinity favor the precipitation of carbonate cements (Worden and Matray., 1998; Morad et al., 2010). Hydrothermal fluid invasion and the subsequent

* Corresponding author. National Key Laboratory of Petroleum Resources and Engineering, China University of Petroleum (Beijing), Beijing, 102249, China.
** Corresponding author. National Key Laboratory of Petroleum Resources and Engineering, China University of Petroleum (Beijing), Beijing, 102249, China.
E-mail addresses: sfzhu@cup.edu.cn (S. Zhu), 215301734@qq.com (H. Cui).

https://doi.org/10.1016/j.marpetgeo.2025.107513
Received 1 April 2025; Received in revised form 30 May 2025; Accepted 12 June 2025
Available online 16 June 2025

cooling-decompression process are key factors providing these conditions. Hydrothermal fluids migrate from deep to shallow reservoirs via diapirs or major faults, leading to energy and material exchange with the surrounding rock and sediments. This process alters the temperature and pressure conditions of the strata and introduces substantial amounts of deep-sourced materials, thereby accelerating carbonate mineral precipitation (Zhu et al., 2019b; Cui et al., 2022; Liang et al., 2024). Consequently, fault zones facilitating upward fluid migration, as well as areas surrounding and overlying igneous intrusions, are the primary loci of hydrothermal carbonate cementation (Lafay et al., 2017; Su et al., 2022; Cui et al., 2024).

Around 45 Ma, the New Pacific Plate subducted in a WNW direction beneath the Eurasian Plate. During subduction, dehydration of the mantle transition zone facilitated partial melting in the overlying mantle wedge, promoting the upwelling of hydrous mantle material into the asthenosphere. Subsequently, lithospheric delamination triggered large-scale upwelling of mantle-derived hot materials, resulting in intense rifting throughout the Bohai Bay Basin, accompanied by large-scale magmatic and metallogenic activities (Liang et al., 2016; Wang et al., 2022).

As an important component of the Bohai Bay Basin, the Dongying Depression experienced multistage magmatic activity during the deposition of the Shahejie Formation, influenced by the Cenozoic subduction of the New Pacific Plate beneath the eastern margin of the North China Craton. Basaltic magmas derived from the asthenospheric mantle were emplaced within the study area in the form of multiple stages of dikes and sills (Wu et al., 2006; Li et al., 2014). Hence, the Shahejie Formation contains numerous basalt interlayers and preserves distinct hydrothermal alteration signatures (Li et al., 2024b; Zhu et al., 2025). Hydrothermal activities in the Shahejie Formation of the Dongying Depression are primarily concentrated near deep faults or in regions rich in volcanic rocks (Jin et al., 2004; Liang et al., 2024). These hydrothermal activities have a profound impact on the diagenesis of clastic sediments (Menezes et al., 2019), particularly the precipitation and transformation of carbonate minerals. For example, under the influence of hydrothermal fluids, minerals such as calcite, dolomite, and aragonite undergo dissolution, reprecipitation, and replacement (Menezes et al., 2019; Su et al., 2022). Moreover, the infiltration of hydrothermal fluids also promotes the formation of hydrothermal minerals with crystallization temperatures 5–10 °C higher than ambient temperatures (Machel and Lonnee, 2002), such as ankerite, saddle dolomite, ammonium dawsonite, apatite, and gypsum. The presence of these hydrothermal minerals and mineral assemblages serves as direct evidence of hydrothermal activity (Mills and Elderfield, 1995). Petrographic observation, isotopic analysis, fluid inclusion microthermometry, and *in situ* U-Pb isotopic dating of calcite provide critical constraints into the timing, origin, migration pathways, and spatial distribution of the hydrothermal fluids (Smith and Davies, 2006; Yang et al., 2022; Li et al., 2023).

Previous studies have demonstrated the presence of hydrothermal activity in the Eocene Shahejie Formation of the Dongying Depression through petrographic and mineralogical analyses. Evidence includes hydrothermal mineral assemblages such as fluorite-anhydrite-pyrite-quartz, anhydrite-barite (Li and Li, 2016), kaolinite-dolomite (Li and Li, 2017), and dolomite-calcite-apatite (Hou et al., 2019), as well as core features like mudstone bleaching and thermal fracturing features (Hou et al., 2019). Additionally, previous studies have investigated the impact of hydrothermal fluids on reservoir diagenesis and source rock maturation (Li et al., 2024b). In summary, ample evidence demonstrates the strong influence of hydrothermal fluid activity on the diagenesis and reservoir evolution of the Eocene Shahejie Formation. However, the timing, duration, and spatial extent of hydrothermal fluid activity, as well as the material sources and formation mechanisms of hydrothermally influenced carbonate cements, remain relatively underexplored.

Therefore, this study comprehensively employs petrographic and mineralogical techniques (thin section observation, scanning electron microscopy, electron probe microanalysis, cathodoluminescence) and geochemical methods (fluid inclusion microthermometry) to examine the mineralogical composition, morphology, stage, distribution, and formation mechanisms of hydrothermally derived carbonate cements in the Eocene Shahejie Formation sandstone reservoirs of the Dongying Depression. Additionally, *in situ* U-Pb isotopic dating of calcite is employed to constrain the timing of hydrothermal fluid migration, providing supplementary evidence to existing theories on the evolution of hydrothermal fluids in the Dongying Depression. The specific objectives of this study are as follows: 1) to identify petrographic and geochemical evidence of hydrothermal fluid influence on the Eocene Shahejie Formation sandstones in the Dongying Depression; 2) to investigate the material origin and formation mechanisms of hydrothermally derived carbonate cements; 3) to determine the stages and timing of hydrothermal activity in the Eocene Shahejie Formation of the Dongying Depression.

2. Geological setting

The Dongying Depression is located in the southeastern part of the Jiyang Depression within the Bohai Bay Basin (Fig. 1A and B). It is bounded by the Chenjiazhuang Uplift to the north, the Luxi and Guangrao Uplift to the south, the Qingcheng Uplift to the west, and the Qintuozi Uplift to the east. (Fig. 1C) (Meng et al., 2021). The depression is characterized by the structural features of 'northern faults and southern onlap', and a 'steep northern slope and gentle southern slope', forming a typical asymmetric continental half-graben basin. (Fig. 1D) (Zahid et al., 2016; Yang et al., 2018). Controlled by a series of syn-sedimentary normal faults (Dou et al., 2020), the depression is divided into three zones from north to south: the northern steep slope zone, the central sag zone, and the southern gentle slope zone. The central sag zone comprises the Minfeng, Lijin, Niuzhuang, and Boxing Subsag (Liu et al., 2017). The study area is located in the northern part of the Dongying Depression (Fig. 1C).

During the Mesozoic, the northeastern margin of the Eurasian continent was tectonically dominated by the subduction of the Paleo-Pacific plate, commonly referred to as the Izanagi Plate. This north-to northwest-directed subduction persisted until approximately 50 Ma, when the Izanagi–Pacific spreading ridge was fully subducted beneath the East Asian margin, marking the cessation of Izanagi subduction and initiating a major reorganization of the Pacific Plate's motion (Wu and Wu, 2019; Liu et al., 2020). Following this transition, the New Pacific Plate began to subduct westward at a lower angle, progressively influencing the tectonic evolution of East Asia during the Cenozoic (Xu et al., 2021). Consequently, the hydrothermal processes that influenced the Eocene Shahejie Formation in the northern Dongying Depression of the Bohai Bay Basin are more plausibly linked to regional tectonic reorganization associated with the westward subduction of the New Pacific Plate, rather than to the earlier Izanagi subduction regime.

Within this tectonic background, the Bohai Bay Basin underwent two extensional evolutionary stages during the Mesozoic and Cenozoic eras (Hu et al., 2001), accompanied by significant intermediate and basic magmatic activity. Cenozoic magmatic activity is divided into four stages: from the Kongdian stage to the fourth member of Shahejie stage, the third member of Shahejie stage, from the second member of Shahejie stage to the Dongying stage, and the Guantao stage. Magmatic activity exhibits a spatial pattern of 'more in the east and less in the west, more in the north and less in the south', with volcanic rocks being more concentrated in the Kongdian Formation, the third member of Shahejie Formation, the first member of Shahejie Formation, and Guantao Formation (Fig. 1B) (Jin et al., 2012).

The Cenozoic sedimentary strata in the Dongying Depression are well-preserved, comprising, from bottom to top, the Paleogene Kongdian (E*k*), Shahejie (E*s*), and Dongying Formation (Ed), followed by the Neogene Guantao (E*g*) and Minghuazhen Formation (E*m*) (Feng et al., 2013). Among these, the Shahejie Formation is extensively distributed across the Dongying Depression and is subdivided into four members,

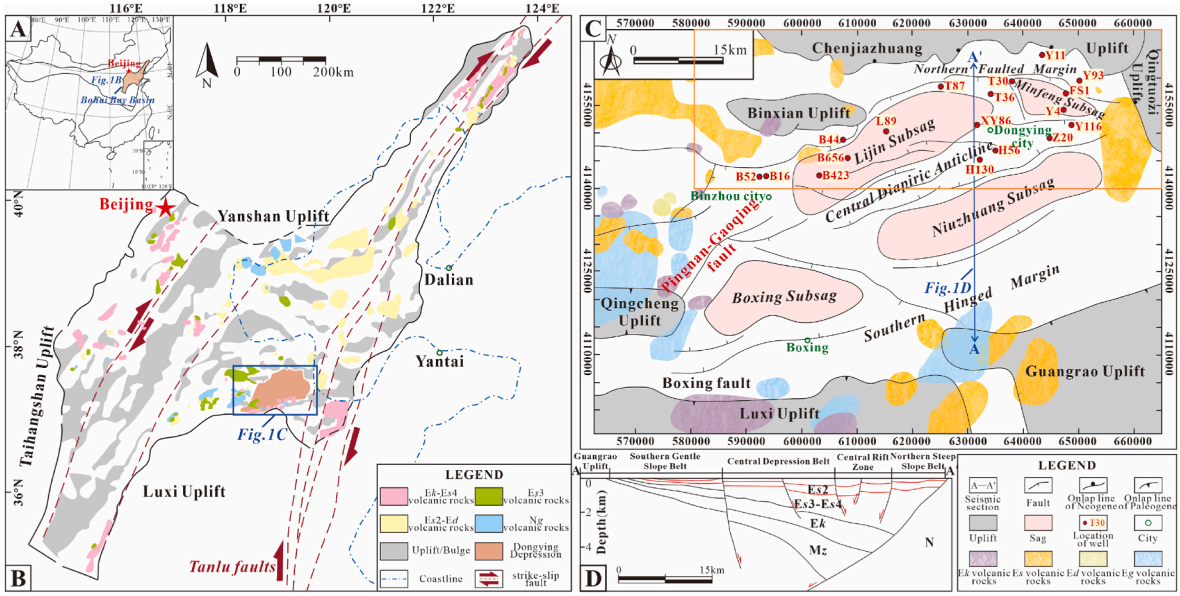

Fig. 1. (A) Location of the Bohai Bay Basin in East China. (B) Tectonic location of the Dongying Depression in the Bohai Bay Basin (modified from Lao et al., 2020; Jin et al., 2012). (C) Schematic map of secondary tectonic units in the Dongying Depression (modified from Lampe et al., 2012; Feng et al., 2013; Meng et al., 2021); and (D) a N-S trending, structural section with the location shown in (C) (Lao et al., 2020; Yang et al., 2023). *Ng*: Guantao Formation (Miocene); *Ed*: Dongying Formation (Oligocene); *Es*1: the first Member of the Shahejie Formation (Oligocene); *Es*2: the second Member of the Shahejie Formation (Eocene-Oligocene); *Es*3: the third Member of the Shahejie Formation (Eocene); *Es*4: the fourth Member of the Shahejie Formation (Eocene); *Ek*: Kongdian Formation (Eocene); *Mz*: Mesozoic Formation.

ranging from *Es*4 at the bottom to *Es*1 at the top. The Eocene Shahejie Formation serves as the primary stratigraphic target for this investigation. After deposition, the formation experienced a brief uplift phase, succeeded by prolonged subsidence. Maximum burial depths range from approximately 1700 m–4600 m, with corresponding paleotemperature of approximately 90–180 °C (Fig. 2) (Chen et al., 2022). The Eocene Shahejie Formation was deposited during the initial stages of major fault development in the Bohai Bay Basin, leading to the rapid deposition of a fan delta system, which includes two subfacies: the pro-fan delta and the fan delta front, as well as steep bank and alluvial plain deposits (Wu et al., 2006). The formation is characterized by interbedded, unevenly thick deposits of mudstone, gravelly sandstone, sandstone, and siltstone

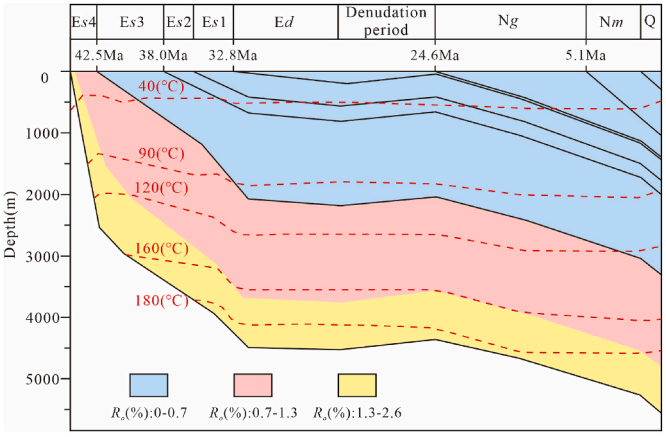

Fig. 2. Simulated burial and thermal history of Well FS1 in the Dongying Depression showing paleoisotherms and Ro values (modified from Chen et al., 2022). Q: Quaternary Formation; *Nm*: Minghuazhen Formation (Pliocene); *Ng*: Guantao Formation (Miocene); *Ed*: Dongying Formation (Oligocene); *Es*1: the first Member of the Shahejie Formation (Oligocene); *Es*2: the second Member of the Shahejie Formation (Eocene-Oligocene); *Es*3: the third Member of the Shahejie Formation (Eocene); *Es*4: the fourth Member of the Shahejie Formation (Eocene).

(Fig. 3).

3. Samples and analytical techniques

3.1. Petrological analysis

This study presents a systematic investigation of reservoir characteristics of the Eocene Shahejie Formation, Dongying Depression, based on 153 subsamples collected from 15 representative core samples. Twenty-one thin sections were prepared to analyze the mineralogical characteristics, spatial distribution, and diagenetic evolution. All thin sections were impregnated with blue epoxy resin to enhance pore visibility, and stained with a mixture of alizarin red-S solution and potassium ferricyanide to differentiate non-iron-bearing carbonate minerals and iron-bearing carbonate minerals. The images were captured using an Olympus BX51 metallographic microscope equipped with the Olympus Stream image acquisition system (Olympus Soft Imaging Solutions GmbH). All images were taken under consistent conditions at a resolution of 4800 × 3600 pixels and stored in JPG format for further analysis at the State Key Laboratory of Petroleum Resources and Prospecting, China University of Petroleum (Beijing).

Following thin section analysis, seven samples were selected to prepare polished thin sections without cover slips for cathodoluminescence (CL) analysis at the State Key Laboratory of Petroleum Resources and Prospecting, China University of Petroleum (Beijing). The CL8200 Mk-2 system from Cambridge Image Technology Limited (CITL, Hatfield, UK) was integrated with a Leica DM2500 microscope (Leica Microsystems, Wetzlar, Germany) equipped with a dedicated camera system to examine luminescence characteristics and compositional variations of carbonate minerals. Due to variations in luminescence intensity across the samples, the exposure time was adjusted between 1 and 8 s to achieve optimal image clarity.

Scanning electron microscope (SEM) observations were conducted on freshly fractured surfaces of sandstone samples, and 21 samples were ultrasonically cleaned in ethanol to remove surface contaminants and fine-grained debris. Secondary electron imaging was performed using an SU8010 field emission scanning electron microscope (FE-SEM; Hitachi

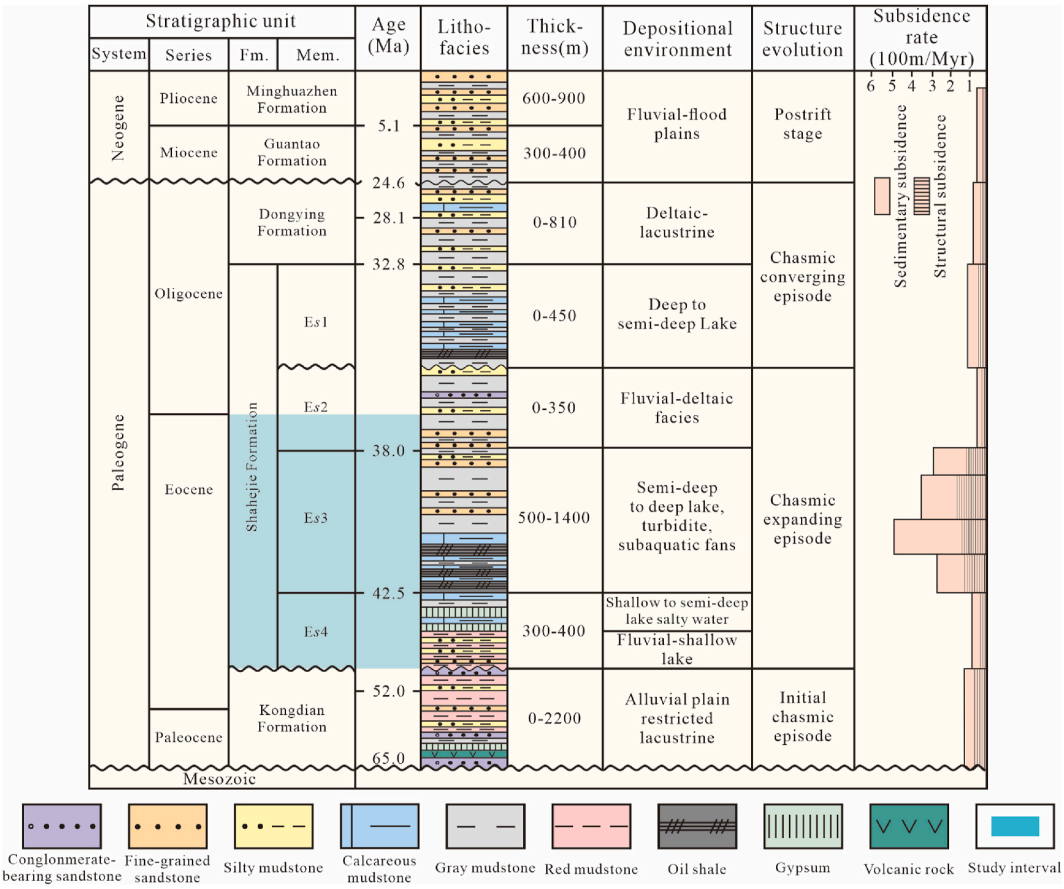

Fig. 3. Stratigraphic column of Dongying Depression (modified from Wu et al., 2022; Ma et al., 2016; Li et al., 2022). Es1: the first Member of the Shahejie Formation (Oligocene); Es2: the second Member of the Shahejie Formation (Eocene-Oligocene); Es3: the third Member of the Shahejie Formation (Eocene); Es4: the fourth Member of the Shahejie Formation (Eocene).

Company, Tokyo, Japan) equipped with an energy dispersive X-ray spectroscopy (EDS) microanalyser. To reduce charging effects and improve image resolution, a conductive gold coating was applied to the freshly fractured rock surfaces. At an acceleration voltage of 20 kV, secondary electron images were acquired at a resolution of 1280 × 960 pixels and stored in TIF format. This part of the work was also carried out at the China University of Petroleum (Beijing).

Quantitative elemental analysis of carbonate cements in six samples was conducted at the School of Civil and Resource Engineering, University of Science and Technology Beijing (USTB), using a JEOL JXA-8100 electron microprobe (JEOL Limited, Tokyo, Japan), operated at 15 kV acceleration voltage, 10 nA beam current, and a beam diameter of approximately 5 μm. The analytical accuracy for major elements was within 1 wt% (weight percent), while that for trace elements was within 3 wt% (weight percent).

3.2. Bulk isotope geochemistry ($\delta^{13}C$ and $\delta^{18}O$)

To constrain the origin and diagenetic environment of carbonate cements, carbon and oxygen isotope compositions were measured on six representative samples characterized by abundant calcite cement at the State Key Laboratory of Petroleum Resources and Prospecting, China University of Petroleum (Beijing). Approximately 0.25–0.30 mg of powdered material was obtained using a micro-spatula and reacted with 2 mL of concentrated orthophosphoric acid (H_3PO_4) in sealed vials at 75 °C for a minimum duration of 5 h to ensure complete liberation of CO_2. The evolved CO_2 was transported using ultra-high purity helium (99.999 %) as a carrier gas to an Isoprime PrecisION isotope ratio mass spectrometer (Elementar, Langenselbold, Germany) for $\delta^{13}C$ and $\delta^{18}O$ analysis. All measurements were calibrated against the international reference material IAEA-CO-8 ($\delta^{13}C = -5.764$ ‰; $\delta^{18}O = -22.7$ ‰), and results are reported in per mil (‰) relative to the Vienna Pee Dee Belemnite (V-PDB) standard. The analytical reproducibility was better than ±0.02 ‰ for both isotopes based on replicate measurements of internal laboratory standards. Detailed sample information and raw isotopic data are presented in Appendix S1.

3.3. Fluid inclusion

Three samples containing carbonate-rich cements were analyzed to determine fluid inclusion homogenization temperatures. The experiments were performed at the Beijing Institute of Uranium Geology Analytical Laboratory (China National Nuclear Corporation, CNNC). To achieve precise measurements (±2 °C), the experiments were conducted using a Linkam THMS-600 heating stage (Linkam Scientific Instruments, Salford, UK; temperature measurement range: 100 to 400 °C) mounted on a Zeiss Axio Imager 2 microscope (Carl Zeiss AG, Oberkochen, Germany). Before the measurements, fluid inclusions in the calcite crystals were observed on doubly polished thin sections (100 μm thick) to determine the size, shape, orientation, and liquid-to-gas ratio. During heating, the temperature ramp rate was initially set at 10 °C/min and then reduced to 1–2 °C/min as the phase transition point was approached. During cooling, the fluid inclusions were frozen completely, then reheated at a rate not exceeding 0.5 °C/min. Images (2592 × 1944 pixels) were captured and stored in JPG format. It is important to note that during the systematic measurements of homogenization temperatures from low to high, precautions were taken to avoid overheating and stretching of the inclusions, and non-

reproducible results were excluded from the analysis (Zhu et al., 2019a).

3.4. Carbonate U-Pb geochronology

To conduct a geochronological study of carbonate cements, two samples were selected for U-Pb analysis and age determination at the Micro-Origin and Spectrum Laboratory (Sichuan Chuanyuan Weipu Analytical Technology Co. Ltd., Chengdu, China). The rock samples were first cut to expose fresh surfaces, which were then embedded in epoxy resin mounts with a diameter of 2.5 cm. The surfaces were polished to meet the analytical requirements. Subsequently, *in situ* U-Pb dating of the carbonate cements was performed using the ASI Resolution LR 193 nm ArF Excimer Laser system in conjunction with a Thermo Scientific Quadrupole iCap TQ Inductively Coupled Plasma Mass Spectrometer (Q-ICP-MS). The procedure was as follows: prior to analysis, the samples were cleaned in an ultrasonic bath with ethanol, and the entire analytical system was flushed with the helium gas. During analysis, manual pre-screening was performed to identify areas with varying U/Pb and $^{207}Pb/^{206}Pb$ isotope ratios. The samples were then ablated in a helium atmosphere. The laser operated in a circular ablation spot with a diameter of 120 μm, a frequency of 15 Hz, and an energy density of 3 J/cm^2.

The data processing methods were based on those of Roberts and Walker (2016) and Nuriel et al. (2019). The $^{207}Pb/^{206}Pb$ and $^{206}Pb/^{238}U$ isotope ratios were normalized using the AHX-1d carbonate standard (independently calibrated to an age of 236.9 ± 1.6 Ma by isotope dilution; Zhao et al., unpublished data). Cross-validation was performed using the LD-5 (72.5 ± 1.0 Ma; Wu et al., 2024) and Duff (~64 Ma; Hill et al., 2016) carbonate standards to ensure the accuracy and reliability of the results. After the analysis, the data from all test samples were plotted on a Tera-Wasserburg Concordia diagram using the Isoplot plugin to calculate the final isotopic age.

4. Results

4.1. Framework composition

According to the classification scheme of Folk (1974), the Eocene Shahejie Formation sandstones in Dongying Depression are primarily lithic feldspathic sandstones, followed by lithic sandstones, feldspathic lithic sandstones, feldspathic sandstones, and a minor proportion of feldspathic quartz sandstones (Fig. 4A). The mineralogical framework composition is $Q_{48.2}F_{24.2}R_{27.6}$. Detrital quartz content ranges from 25.2 % to 78.1 %, with monocrystalline quartz being predominant (Fig. 5A–F). The feldspar content ranges from 3.3 % to 60.7 %, with typical Carlsbad twin features observable under cross-polarized light (Fig. 5F). The lithic fragment content ranges from 2.1 % to 47.8 %, with metamorphic lithic fragments being the most abundant type, accounting for approximately 48.9 % of the total lithic fragments. In addition, the lithic fragments include 33.9 % volcanic lithic fragments and 17.2 % sedimentary lithic fragments (Fig. 4B). The volcanic lithic fragments are mainly composed of extrusive lithic fragments, while the sedimentary lithic fragments are predominantly shale fragments.

4.2. Diagenetic minerals

4.2.1. Calcite

The carbonate cements in the Eocene Shahejie Formation, Dongying Depression, exhibit a relatively simple composition. Under polarized light microscopy, alizarin red-stained calcite cement occupies a substantial portion of the intergranular space, with no observation of siderite, dolomite, or ankerite (Fig. 5A–F). These calcite cements exist in two forms: one as block calcite cement and the other as scattered patchy calcite.

Blocky calcite cement: Blocky calcite cement is commonly observed in sandstones with low matrix content, where the clastic particles are distributed in a 'floating' arrangement with minimal contact between them (Fig. 5A–C). The crystals of blocky calcite cement are relatively coarse with well-developed cleavage (Fig. 5D). Under cathodoluminescence, these cements exhibit an orange-red luminescence, without distinct indications of different cementation generations (Fig. 5I and J). These calcite cements almost completely fill the pore spaces, resulting in very low porosity.

Scattered patchy calcite: Scattered patchy calcite primarily fills the intergranular pores in matrix-rich sandstones, where the clastic particles are in point contact with one another (Fig. 5E and F). Compared to blocky calcite cement, scattered patchy calcite has significantly smaller crystal sizes due to the limited space available for growth (Fig. 5G). Under cathodoluminescence, scattered patchy calcite also exhibits an orange-red luminescence without distinct indications of cementation generations (Fig. 5K and L).

Chemical composition of carbonate cements: To investigate the differences in the chemical composition of calcite cements in different forms, electron probe microanalysis was conducted on 11 carbonate cement spots from 4 sandstone samples. The results reveal that blocky calcite cements (Fig. 6A–D) and scattered patchy calcite (Fig. 6E) are primarily composed of $CaCO_3$, with very low contents of Mg, Fe, and Mn. The molar percentages of the components are as follows: $CaCO_3$:

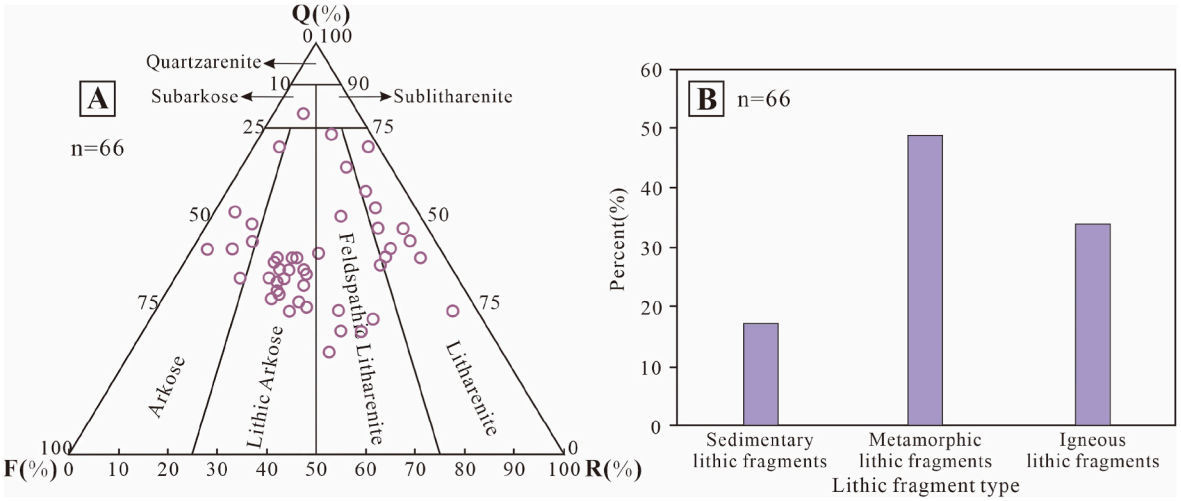

Fig. 4. (A) Q-F-R (quartz-feldspar-rock) triangular diagram of sandstone petrography showing the composition of the Eocene Shahejie Formation (E*s*). (B) Histogram of different types of debris content of the Eocene Shahejie Formation (E*s*).

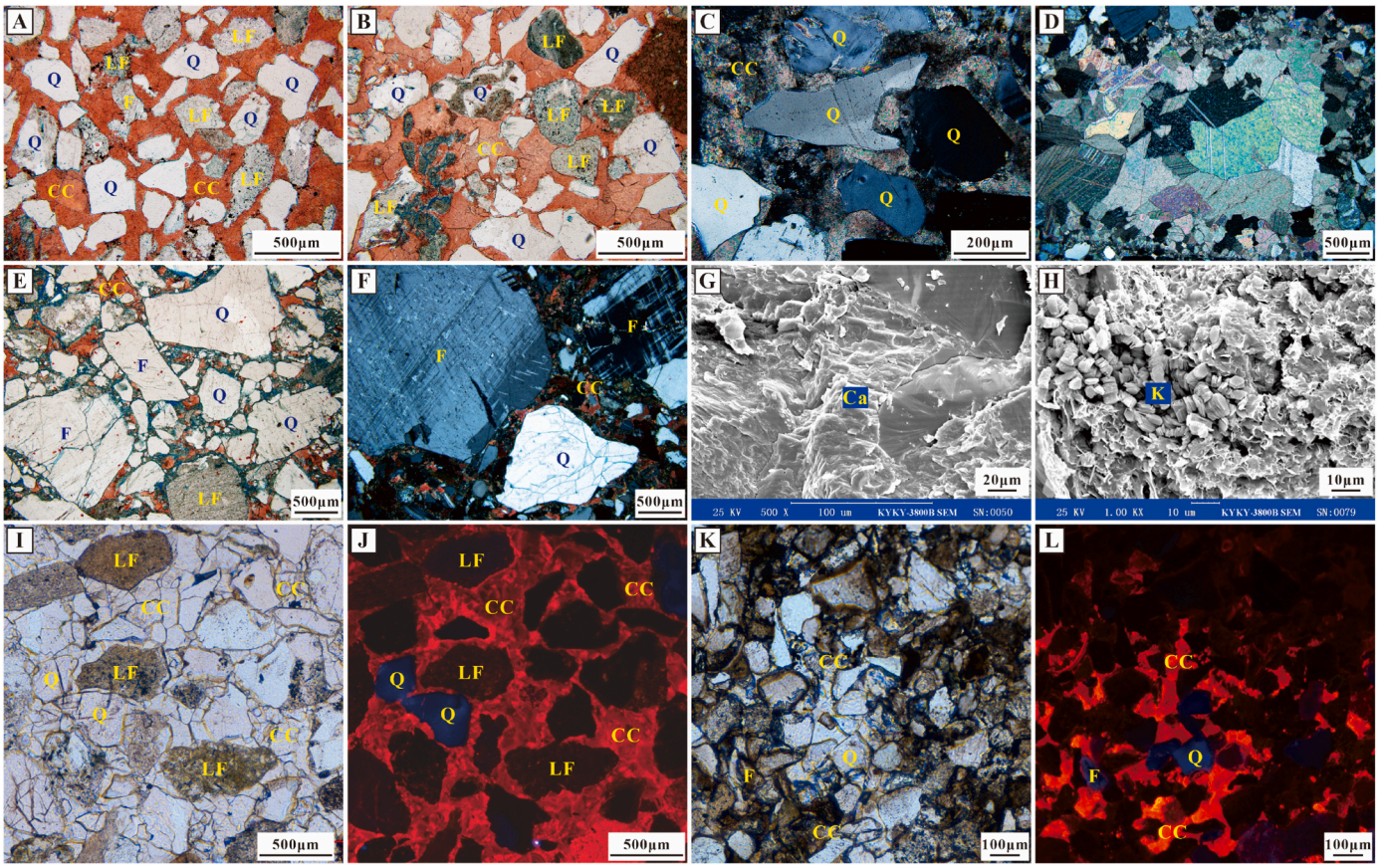

Fig. 5. (A) Almost all pores are filled with blocky calcite, resulting in extremely low surface porosity. Well H56, Es, 2034 m, PPL. (B) Blocky calcite cement is commonly observed in matrix-poor sandstones, appearing red upon staining. Well T36, Es, 2019.6 m, PPL. (C) Calcite displays the high white interference color under cross-polarized light. Well Z20, Es, 2077.9 m, XPL. (D) Blocky calcite cement with well-developed cleavage. Well Z20, Es, 2077.9 m, XPL. (E)Scattered patchy calcite filling intergranular residual pores. Well T30, Es, 1842.6 m, PPL. (F) Feldspar with Carlsbad twins. Well Y11, Es, 1370.9 m, XPL. (G) Calcite cement filling intergranular pores. Well Z20, Es, 2100.3 m, SEM. (H) Worm-like kaolinite filling secondary pores. Well Z20, Es, 2166.75 m, SEM. (I) Well-developed blocky calcite cement. Well T36, Es, 2019.6 m, PPL. (J) Blocky calcite cement presents as deep orange-red under cathodoluminescence (CL) observation. Well T36, Es, 2019.6 m, CL. (K) Well-developed scattered patchy calcite. Well Z20, Es, 2074.6 m, PPL. (L) Scattered patchy calcite presents as deep orange-red under CL observation. Well Z20, Es, 2074.6 m, CL. CC: calcite cement; F: feldspar; K: kaolinite; LF: lithic fragment; PPL: plane-polarized light; Q: quartz; SEM: scanning electron microscopy; XPL: cross-polarized light.

92.18 %–98.15 %; $MgCO_3$: 0.45 %–2.80 %; $FeCO_3$: 0.64 %–2.34 %; $MnCO_3$: 0.17 %–2.86 %. The average chemical composition is expressed as $Ca_{0.964}Mg_{0.013}Fe_{0.013}Mn_{0.011}CO_3$ (Fig. 7).

Distribution of carbonate cements: The sandstones of the Eocene Shahejie Formation in Dongying Depression can be classified into two types on rock maturity: matrix-rich sandstones and matrix-poor sandstones. These two types exhibit significant differences in the development of carbonate cements. Matrix-rich sandstones typically display poor sorting and a high content of intergranular matrix, indicating low maturity. Carbonate cement is either absent or sparsely present, filling a small amount of the pore spaces between the grains. In contrast, matrix-poor sandstones are well sorted with low matrix content, exhibiting abundant blocky calcite cement under the microscope (Fig. 8). Therefore, carbonate cement is more extensively developed in well-sorted sandstones with lower matrix content and higher maturity.

4.2.2. Authigenic kaolinite

Authigenic kaolinite appears as loosely packed crystals with widely developed intercrystalline pores, largely filling secondary porosity in a loose arrangement. Scanning electron microscopy (SEM) observations reveal that the size of kaolinite stacks is uniform, predominantly ranging from 5 to 10 μm in diameter (Fig. 5H). A small proportion of kaolinite results from feldspar alteration and adheres to grain surfaces. Dissolution of carbonate minerals is evident between kaolinite crystals, indicating that the formation of authigenic kaolinite postdates carbonate cementation.

4.2.3. Barite

Under plane-polarized light, barite exhibits two nearly perpendicular cleavage sets (Fig. 9A and C), while under cross-polarized light, it exhibits a grayish-white interference color (Fig. 9B and D). Electron probe microanalysis reveals that the primary composition of barite is $BaSO_4$ (Fig. 6F). Barite is predominantly found near fault zones, with small amounts of authigenic kaolinite observed in its dissolution pores. Notably, in areas with significant barite development, no calcite cement is present. These findings suggest that barite precipitation occurred prior to kaolinite formation, and barite does not coexist with calcite cement.

4.2.4. Dawsonite

Microscopically, dawsonite is colorless and transparent, exhibiting a high white interference color (Fig. 9E and F). Most unit crystals show single radial structures ranging from 10 to 50 μm in length and 1–5 μm in diameter (Fig. 9G). Aggregates are commonly formed by connecting multiple radial unit crystals. The dawsonite forms around the calcite, from the edge to the inside (Fig. 9F), indicating that the dawsonite forms after calcite. Additionally, dawsonite locally exhibits selective replacement of feldspar along cleavage planes and quartz along microfractures (Fig. 9H).

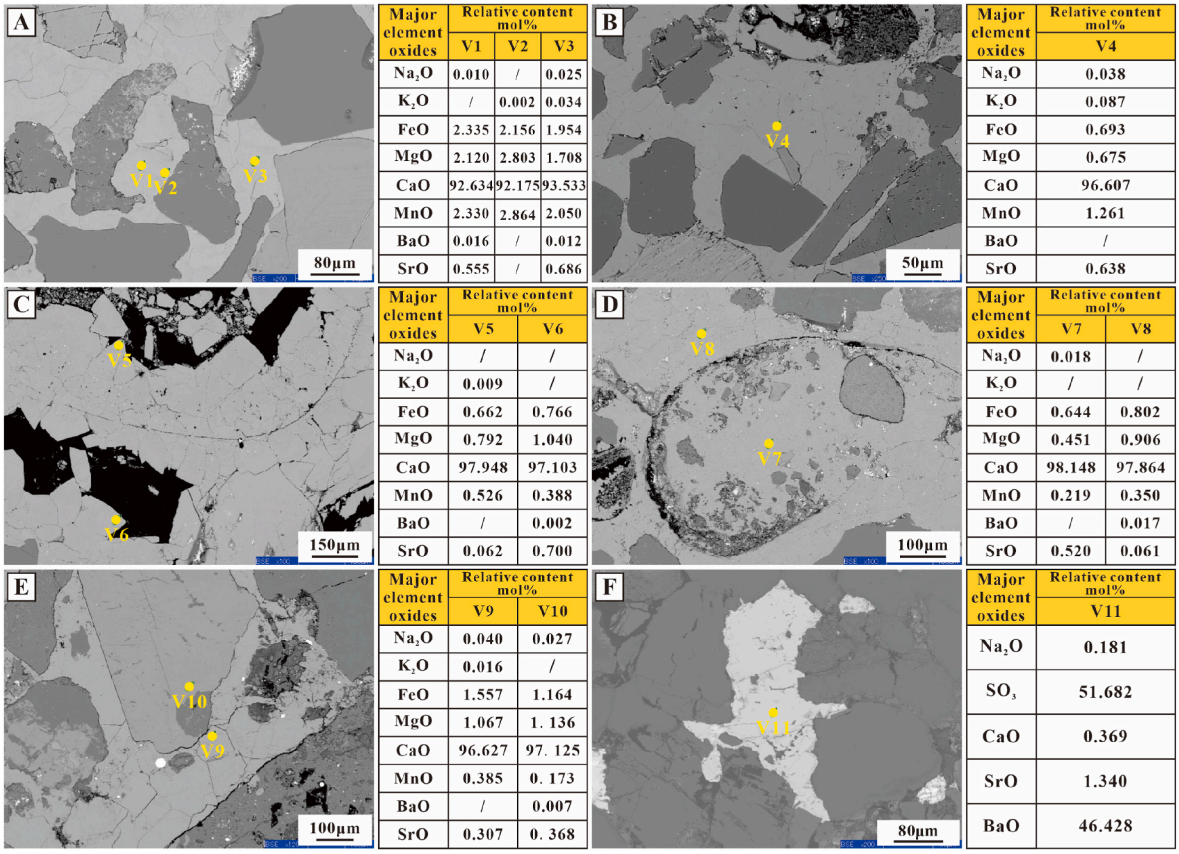

Major element oxides	Relative content mol% V1	V2	V3
Na_2O	0.010	/	0.025
K_2O	/	0.002	0.034
FeO	2.335	2.156	1.954
MgO	2.120	2.803	1.708
CaO	92.634	92.175	93.533
MnO	2.330	2.864	2.050
BaO	0.016	/	0.012
SrO	0.555	/	0.686

Major element oxides	Relative content mol% V4
Na_2O	0.038
K_2O	0.087
FeO	0.693
MgO	0.675
CaO	96.607
MnO	1.261
BaO	/
SrO	0.638

Major element oxides	Relative content mol% V5	V6
Na_2O	/	/
K_2O	0.009	/
FeO	0.662	0.766
MgO	0.792	1.040
CaO	97.948	97.103
MnO	0.526	0.388
BaO	/	0.002
SrO	0.062	0.700

Major element oxides	Relative content mol% V7	V8
Na_2O	0.018	/
K_2O	/	/
FeO	0.644	0.802
MgO	0.451	0.906
CaO	98.148	97.864
MnO	0.219	0.350
BaO	/	0.017
SrO	0.520	0.061

Major element oxides	Relative content mol% V9	V10
Na_2O	0.040	0.027
K_2O	0.016	/
FeO	1.557	1.164
MgO	1.067	1. 136
CaO	96.627	97. 125
MnO	0.385	0. 173
BaO	/	0.007
SrO	0.307	0. 368

Major element oxides	Relative content mol% V11
Na_2O	0.181
SO_3	51.682
CaO	0.369
SrO	1.340
BaO	46.428

Fig. 6. Photomicrographs and electron probe microanalysis (EPMA) results of carbonate cements and barite. Yellow solid circles indicate the areas analyzed by electron microprobe. (A) Blocky calcite cement. Well T36, Es, 2019.6 m, EPMA. (B) Blocky calcite cement. Well Z20, Es, 2075.84 m, EPMA. (C) Blocky calcite cement. Well Z20, Es, 2077.9 m, EPMA. (D) Blocky calcite cement. Well Z20, Es, 2077.9 m, EPMA. (E) Scattered patchy calcite. Well Y93, Es, 1808.85 m, EPMA. (F) Barite. Well B44, Es, 2103.4 m, EPMA. EPMA: electron probe microanalysis.

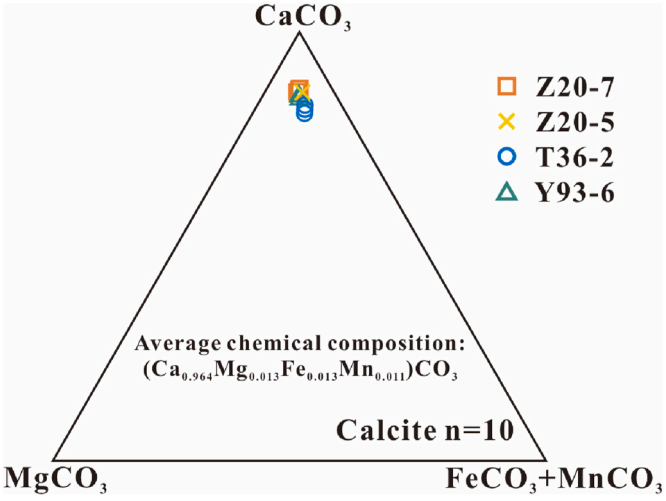

Fig. 7. Major element composition of carbonate cements in the Eocene Shahejie Formation, Dongying Depression.

4.3. Fluid inclusion thermometry

As calcite precipitated, a large number of fluid inclusions were captured. In three samples, 24 aqueous inclusions containing a vapor bubble were found within blocky calcite cement and scattered patchy calcite, and their homogenization temperatures were measured. Almost all inclusions exhibit a gas-liquid phase ratio distribution of ≤10 %, with individual inclusions reaching 15 % or 20 %. These inclusions displayed elongated, elliptical, rounded, and, less commonly, irregular crystal shapes, with diameters ranging from 2 to 16 μm. The majority of them are distributed in clusters or zones (Fig. 10A–D). It is challenging to determine the origin of these fluid inclusions and to define fluid inclusion assemblages (FIAs) in these calcite crystals because no growth banding is evident. However, most fluid inclusions appear to be primary, as they are clustered with varying abundances within these calcite crystals, which may be related to growth zonation (Goldstein and Reynolds, 1994). Inclusions that are isolated or distributed along microfractures are likely secondary and were therefore excluded from further analysis.

Basal or completely porous calcite cements are typically considered to have precipitated during shallow burial stages at relatively low paleotemperatures (Zhu et al., 2019b). However, the microthermometric data from the fluid inclusions in this study show homogenization temperatures ranging from 85 to 350 °C, with an average of 195.08 °C (Fig. 10E), significantly higher than the geothermal conditions of the corresponding strata at that time.

4.4. Isotope geochemistry

The $\delta^{18}O$ and $\delta^{13}C$ values were obtained for the carbonate cements of six samples from five cored wells (Fig. 11; Appendix. S1). Carbonate cement $\delta^{18}O$ values exhibit a narrow range from −14.0 to −11.1 ‰ VPDB (Vienna PeeDee Belemnite), with an average of −12.5 ‰, indicating a relatively homogeneous oxygen isotope composition. In contrast, the values of $\delta^{13}C$ show a broader distribution, ranging from −11.8 to −3.1 ‰ VPDB, with an average of −6.6 ‰.

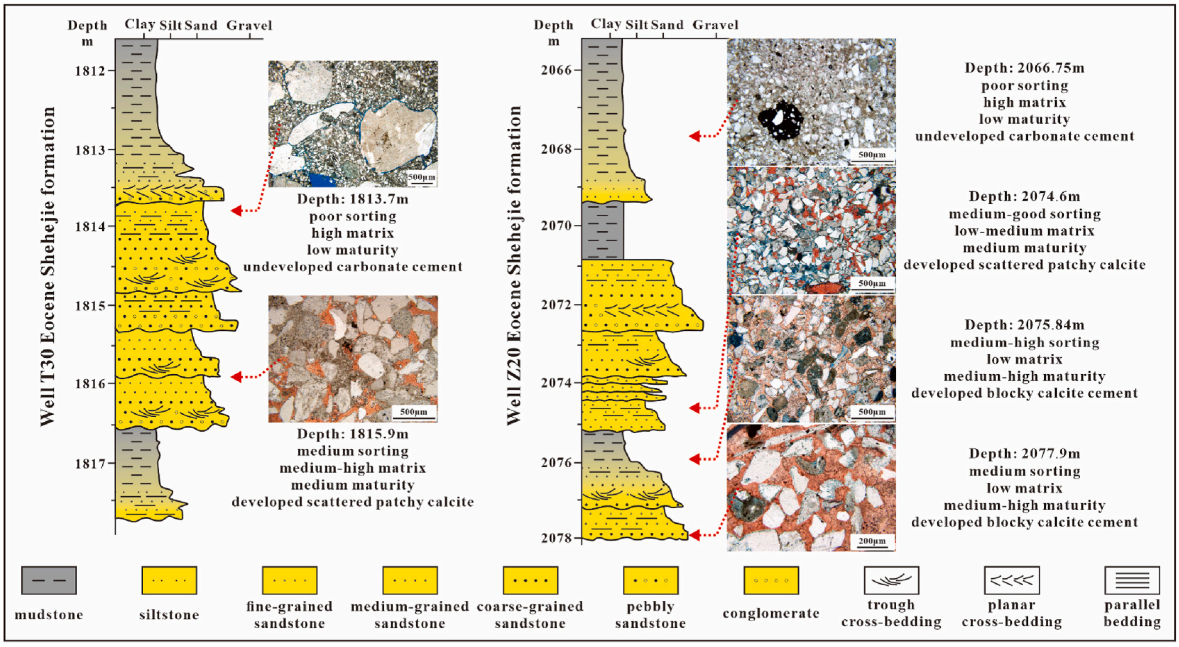

Fig. 8. Vertical distribution characteristics of carbonate cement in Well T30 and Well Z20, Eocene Shahejie Formation. Sandstones with low maturity (poor sorting and abundant matrix) exhibit scattered patchy calcite, whereas sandstones with high maturity (well-sorted and low matrix content) contain well-developed blocky calcite cement.

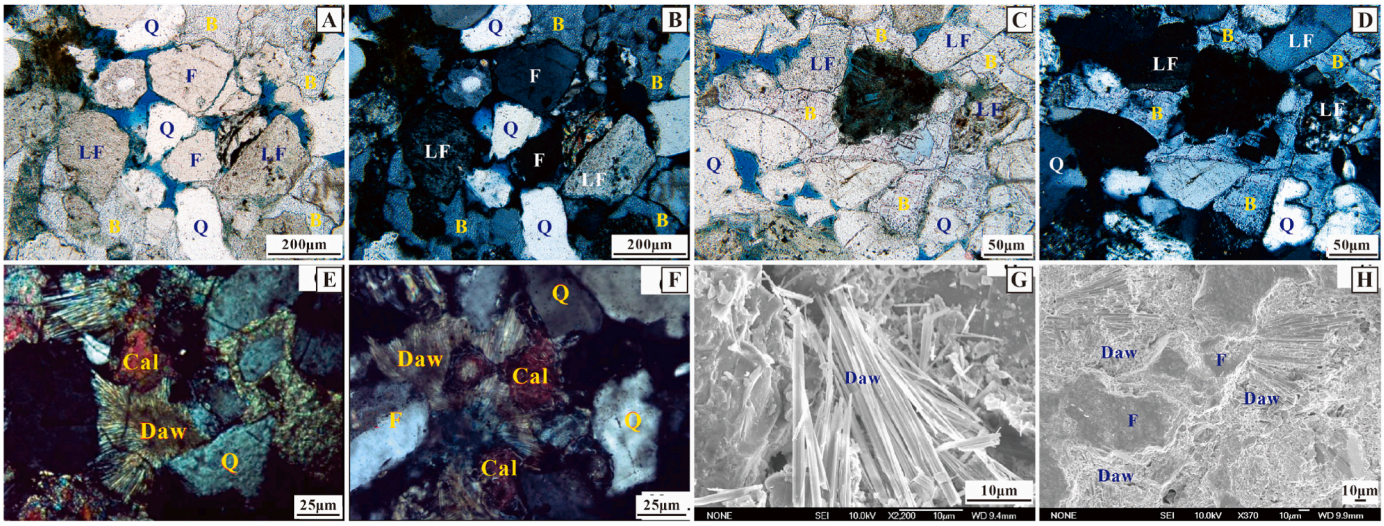

Fig. 9. Typical microscopic and SEM images of barite and dawsonite. (A) Barite filling secondary pores. Well B44, Es, 2103.4 m, PPL. (B) Same view as in (A), with barite showing grayish-white interference color. Well B44, Es, 2103.4 m, XPL. (C) Barite displays two sets of nearly perpendicular cleavage. Well B44, Es, 2103.4 m, PPL. (D) Same view as in (C), with barite showing grayish-white interference color. Well B44, Es, 2103.4 m, XPL. (E) Dawsonite radiates outward and fills in the matrix. Well B52, Es, 1498 m, XPL (Li and Li, 2016). (F) The dawsonite forms around the calcite, from the edge to the inside, collectively filling intergranular pores. Well B52, Es, 1615.1 m, XPL (Li and Li, 2016). (G) The unit crystals of dawsonite appear as single radial structures. Well B16, Es, 1499.1 m, SEM (Li and Li, 2016). (H) Dawsonite fills space left by dissolved K-feldspar. Well B16, Es, 1531.1 m, SEM (Li and Li, 2016). B: barite; Cal: calcite; Daw: dawsonite; F: feldspar; LF: lithic fragment; PPL: plane-polarized light; Q: quartz; SEM: scanning electron microscopy; XPL: cross-polarized light.

4.5. Calcite U-Pb ages

The LA-ICP-MS *in-situ* U-Pb isotopic analysis was performed on two typical calcite cement samples from the study area. A total of 42 analytical spots in the Z20-7 calcite cement sample (n = 42) yielded $^{238}U/^{206}Pb$ and $^{207}Pb/^{206}Pb$ ratios that ranged from 6.02 to 142.0 and 0.21 to 0.84, respectively. The data were integrated with Tera-Wasserburg Concordia diagrams, yielding a lower intercept age for the Z20-7 calcite cement of 39.4 ± 1.9Ma (2σ), with a mean squared weighted deviates (MSWD) of 27 (Fig. 12A).

A total of 154 *in situ* spot analyses of the T36-2 calcite cement sample (n = 154) yielded $^{238}U/^{206}Pb$ and $^{207}Pb/^{206}Pb$ ratios ranging from 0.05 to 5.13 and 0.84 to 0.93, respectively. These U-Pb isotopic data give an isochron age of 42 ± 7.6 Ma (2σ), with the MSWD of 1.2 (Fig. 12B).

5. Discussion

5.1. Hydrothermal evidence

Evidence for hydrothermal activity in Dongying Depression's Eocene

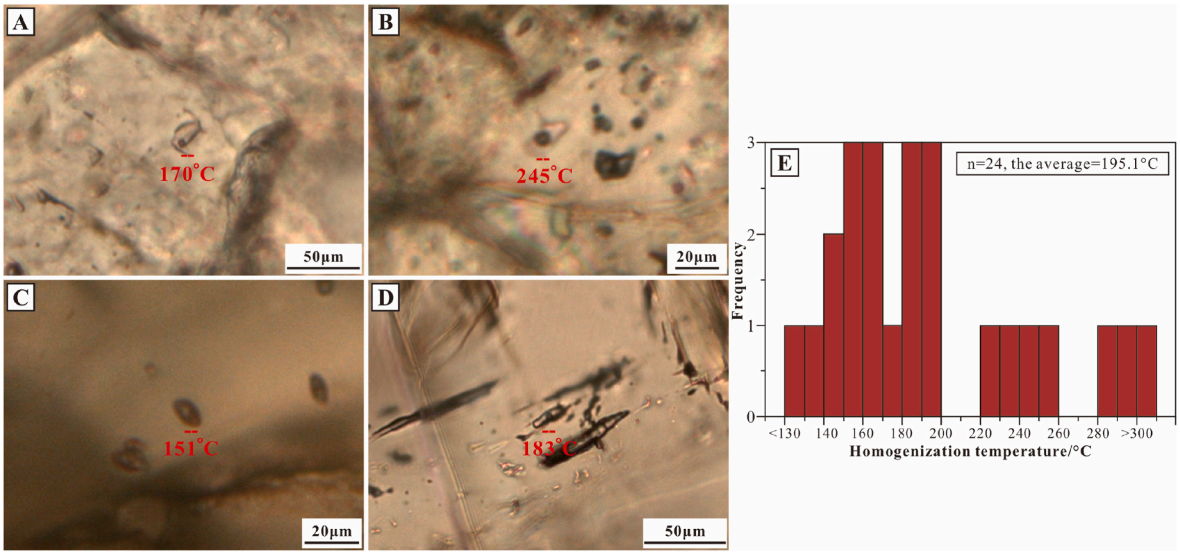

Fig. 10. Photomicrographs of fluid inclusions in the investigated carbonate cements under plane-polarized light (PPL) and histogram of the homogenization temperatures for aqueous inclusions in carbonate cements. (A) Well Z20, Es, 1808.85 m. (B) Well Z20, Es, 1808.85 m. (C) Well T36, Es, 2019.6 m. (D) Well Z20, Es, 2077.9 m. (E) Histogram of homogenization temperatures of carbonate cements.

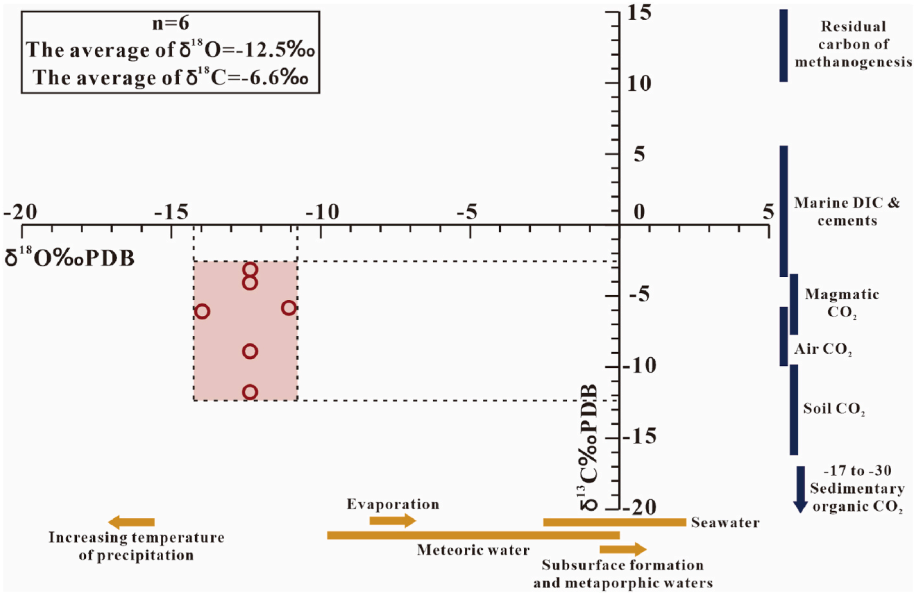

Fig. 11. Cross-plot diagram of $\delta^{18}O$ and $\delta^{13}C$ values of calcite cements from the Shahejie Formation (isotopic signatures and distribution intervals of various fluid flows were from De Boever et al., 2017). The red rectangle represents the concentrated distribution range of all tested samples.

Shahejie Formation is summarized as follows.

1 Magmatic rocks, formed by magma intruding into strata or extruding to the surface and subsequently cooling, are typically associated with the migration of mantle-derived fluids. As such, they serve as direct indicators of hydrothermal processes (Wang et al., 2024). A significant volume of basalt, with a cumulative thickness of approximately 464.1 m, have been identified in the Shahejie Formation along the Gaoqing-Pingnan fault zone in the Dongying Depression (Li et al., 2024a).
2 The formation of barite is typically associated with reactions between deep-seated, barium-rich hydrothermal fluids and sulfate-bearing fluids (Urabe and Kusakabe., 1990; Hein et al., 2007). This mineral is commonly found in low-temperature hydrothermal veins. Additionally, previous studies have shown that the carbon dioxide required for the formation of dawsonite in the Shahejie Formation of the Dongying Depression originates from Cenozoic magmatic-hydrothermal activities ((Li and Li, 2016; Li et al., 2024b). Therefore, the occurrence of hydrothermal minerals such as barite and dawsonite serves as an important indicator of hydrothermal activity.
3 Abnormal homogenization temperatures of fluid inclusions can serve as an important indicator of hydrothermal fluid activity (Davies and Smith., 2006; Yan et al., 2023). The homogenization temperatures of fluid inclusions in the carbonate cement of sandstones from the Eocene Shahejie Formation, Dongying Depression, are significantly higher than typical paleotemperatures. This result clearly indicates that the formation of these carbonate cements was notably influenced by deep hydrothermal activity.

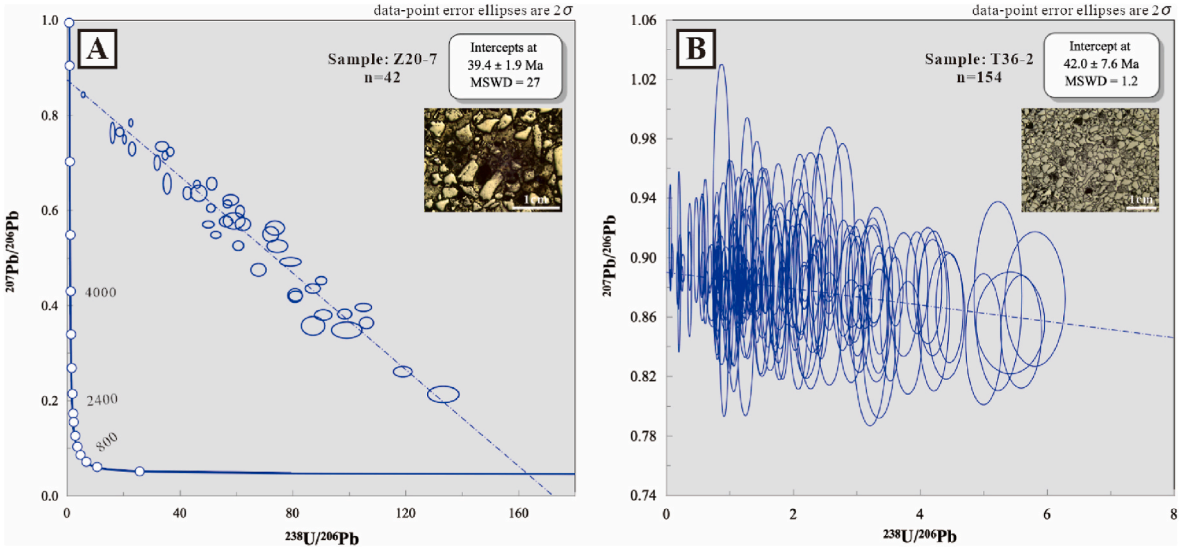

Fig. 12. Tera-Wasserburg Concordia plots showing $^{238}U/^{206}Pb$ versus $^{207}Pb/^{206}Pb$ for the calcite cements. (A) Well Z20, Es, 2077.9 m. (B) Well T36, Es, 2019.6 m. Please see Appendix S2 for the detailed data and laser beam point locations.

4 The Cenozoic gas reservoirs in the Dongying Depression primarily contain three types of mantle-derived gases: CO_2, Ar, and He (Li and Li, 2017; Liang et al., 2024). This indicates that the strata connected to deep, major faults, such as the Gaoqing-Pingnan fault (Fig. 1C), have been influenced by mantle-derived fluids, providing strong evidence for the existence of hydrothermal activity.

5 Previous research has demonstrated that decreases in $\delta^{18}O$ values within carbonate cements are commonly associated with elevated precipitation temperatures during progressive burial (Śliwiński et al., 2016). In this study, the notably low $\delta^{18}O$ values (ranging from −14.0 ‰ to −11.1 ‰) observed in carbonate cements are interpreted as a geochemical signature of high-temperature fluid influence, most likely of hydrothermal origin.

5.2. *Timing and geodynamic setting for hydrothermal fluid flow*

Petrographic observations of clastic rocks from the Eocene Shahejie Formation in Dongying Depression have documented numerous mineralogical and petrographic evidences related to hydrothermal activity in previous studies. These include typical hydrothermal mineral associations such as fluorite-anhydrite-autogenic pyrite-quartz, anhydrite-barite (Li and Li, 2016), muscovite-sodalite-dolomite (Li and Li, 2017), and dolomite-calcite-apatite (Hou et al., 2019). Additionally, core samples display characteristic features such as mudstone bleaching and rock thermal fracturing structures (Hou et al., 2019), confirming the existence of hydrothermal activity. Subsequent studies have examined the geochemical characteristics of rocks altered by hydrothermal fluids, revealing an enrichment of light rare earth elements (LREEs) and a depletion of heavy rare earth elements (HREEs), with δ_{Eu} values showing a distinct positive anomaly. Moreover, the T_{max} and R_o values of source rocks influenced by hydrothermal fluids were significantly elevated. These findings provide the geochemical evidence supporting the role of hydrothermal fluids (Li et al., 2024a). In addition, the mantle-derived CO_2 gas reservoirs distributed in the Dongying Depression have also been confirmed to be closely related to hydrothermal activity (Zeng et al., 2004; Li and Li, 2017; Liang et al., 2024). These results collectively indicate that hydrothermal activity during the deposition of the Eocene Shahejie Formation in the study area is both objectively present and widespread.

The Bohai Bay Basin is located on the southeastern margin of the Eurasian Plate, adjacent to the Pacific Plate, the Indian Ocean Plate, and the Philippine Plate. As a result, its tectonic evolution has been largely controlled by the relative motions of these neighboring plates, with the influence of the Pacific Plate being the most significant. Around 45 Ma, the subduction direction of the New Pacific Plate relative to the Eurasian Plate shifted from north-northwest to northwest-west, accompanied by a significant increase in subduction rate, resulting in enhanced slab rollback and mantle wedge convection beneath East China (Liang et al., 2016; Zhu et al., 2021; Xu et al., 2021). Numerical deformation reconstructions further reveal that the Bohai Bay Basin underwent its most significant extensional deformation between 42 and 32.8 Ma, which facilitated fault reactivation, deep fluid circulation, and increased geothermal gradients-key conditions for hydrothermal fluid migration (Zhu et al., 2021). Additionally, thermal history reconstruction based on apatite fission-track (AFT) and (U-Th)/He thermochronology from the Bohai Bay Basin reveals that the regional heat flow reached a second peak of approximately 80 mW/m^2 during the Late Eocene. This elevated heat flow is interpreted as a manifestation of intensified lithospheric thermal input, likely related to crustal thinning and asthenospheric upwelling driven by the westward subduction of the Pacific Plate (Chang et al., 2018). This temporal correlation provides strong evidence that the regional heat source required for hydrothermal carbonate formation were established during this critical interval. The subduction of the Pacific Plate led to crust and lithosphere thinning, upwelling of the asthenospheric mantle, and triggered surface extension, subsidence, and magmatic activities. As an important part of the Bohai Bay Basin, the Dongying Depression was significantly impacted by the upwelling of thermal materials resulting from the Cenozoic subduction of the New Pacific Plate during the deposition of the Eocene Shahejie Formation. This resulted in exceptionally intense hydrothermal fluid activity within the depression, which in turn influenced the diagenetic evolution of the ancient sediments of the Shahejie Formation. Based on the geological background, this study suggests that the hydrothermal fluids in the study area may be products associated with volcanic activity triggered by the subduction of the New Pacific Plate. Although the exact genesis of the hydrothermal upwelling remains speculative, this interpretation is highly reasonable when considering the regional geological context and existing evidence.

The deep major fault zones serve as primary conduits for the upward migration of deep-seated materials, with magma and associated hydrothermal fluids typically erupting or intruding along these faults (Barbieri et al., 2020). The distribution of such faults is closely coupled with the spatial extent of hydrothermal fluid activity, as fault systems directly influence fluid distribution within the basin. Multiple phases of

magmatic activity in the Dongying Depression during the Cenozoic reflect the continuous release of deep materials toward the surface. Seismic data analysis reveals a distinct fault-controlled distribution of magmatic rocks within the basin (Luo et al., 2020), and mantle-derived CO_2 is also found to be distributed along fault zones (Zeng et al., 2004; Li and Li, 2017). These observations indicate that the fault and fracture systems within the Dongying Depression provide favorable geological conditions for the migration of deep-seated materials, with the Gaoqing-Pingnan fault acting as a key conduit for deep-sourced material transfer and directly controlling the spatial distribution of hydrothermal activity. The Gaoqing-Pingnan fault, located in the western part of the Dongying Depression, displays an "S" shape, with an overall NE-SW trend and a length exceeding 60 km (Zeng et al., 2004). This fault extends from the shallow crust and continues downward into the low-velocity body of the mid-crust, making it a key basal fault that plays a pivotal role in the structural evolution of the Dongying Depression. The fault began developing during the Kongdian Formation deposition and reached its peak activity during the third member of the Shahejie Formation, with basaltic eruptions accompanying this period. The fault's activity gradually waned thereafter. A large number of intermediate to basic volcanic rocks and mantle-derived CO_2 gas reservoirs are found in proximity to the fault, confirming the fault's crucial role in facilitating the migration of deep-sourced materials.

Hydrothermal fluids that migrated along deep major fault zones have exerted significant influence on the diagenetic evolution of sediments. In the Eocene Shahejie Formation sandstones within the study area, carbonate cementation is widely developed. The homogenization temperatures of fluid inclusions within these cements range from 85 to 350 °C, indicating a close relationship with hydrothermal activity. Both blocky carbonate cement and scattered patchy calcite are composed of $CaCO_3$. Under cathodoluminescence, they exhibit a uniform color, without multiphase characteristics. This uniformity suggests that the cementation of these calcite cements occurred 'instantaneously' under the influence of hydrothermal fluids. U-Pb geochronological analyses confirm that the hydrothermal cementation took place during the Eocene (39.4 ± 1.9Ma for Sample Z20-7 and 42 ± 7.6Ma for Sample T36-2), which aligns closely with the timing of the New Pacific Plate Cenozoic subduction beneath the Eurasian Plate. However, owing to the relatively low U/Pb ratios, this age result is associated with a relatively large uncertainty. However, such an error range is commonly reported in previous U-Pb dating studies of carbonate minerals in hydrothermal systems (e.g., Roberts et al., 2020; Jin et al., 2021). The main contributing factors include the compositional heterogeneity of hydrothermal carbonates, inherently low uranium concentrations, and potential lead loss, all of which can lead to a certain degree of data scatter in in-situ analyses. Despite the uncertainty, the age result is statistically robust and can still provide a reasonable constraint on the timing of major hydrothermal activity.

In summary, this study suggests that the hydrothermal activity in the Dongying Depression was likely associated with the Cenozoic subduction of the New Pacific Plate, with significant intensity during the deposition of the Eocene Shahejie Formation. As the primary medium for transporting deep-seated materials, hydrothermal fluids were channeled to the target formation through major deep faults, delivering rich materials for the formation of carbonate cements.

5.3. Genesis of carbonate cements

The formation mechanisms of carbonate cements in clastic rock reservoirs have been extensively studied, and the main explanations for their origin include: (1) carbonate minerals precipitate directly from carbonate-oversaturated alkaline waters; (2) meteoric freshwater leaching dissolves calcium-rich detrital grains, leading to localized supersaturation of calcium carbonate, which subsequently precipitates *in situ*; (3) acidic fluids derived from organic acid pyrolysis and decarboxylation dissolve feldspar grains and early carbonate cements, releasing large amounts of Ca^{2+} and CO_3^{2-} into the pore water, leading to carbonate cement precipitation in secondary pores; (4) upwelling of deep hydrothermal fluids brings large amounts of deep-sourced materials, triggering extensive carbonate cement precipitation (Dutton, 2008; Ma et al., 2016; Cui et al., 2023).

In the sandstones of the Eocene Shahejie Formation in the Dongying Depression, the degree of carbonate cementation varies significantly across different regions. In areas distant from faults, the carbonate cement content is markedly lower. Moreover, no dissolution of carbonate clasts was observed in thin section observations, thus ruling out the possibility of meteoric water leaching as the origin of the cementation. Carbonate cements in the sandstones primarily fill primary intergranular pores and formed prior to significant compaction, with no precipitation in secondary dissolution pores. And there is a lack of extensive feldspar and lithic grain dissolution (Fig. 5E and F), indicating that Ca^{2+} released by organic acid-driven dissolution did not play a dominant role in the carbonate cementation processes in this area. Previous studies suggest that during the deposition of the Eocene Shahejie Formation, the Dongying Depression was a typical continental rift saline lacustrine basin (Dou et al., 2020), where the formation waters were rich in Ca^{2+}, providing a substantial source for the precipitation of carbonate cements. As demonstrated in the previous sections, the abnormally high homogenization temperatures of fluid inclusions, along with the presence of hydrothermal minerals such as barite and dawsonite, provide strong evidence that carbonate cementation occurred under high-temperature conditions. Therefore, we propose that the calcium source for the carbonate cements in the Eocene Shahejie Formation sandstones of the Dongying Depression is a mixture of calcium derived from primary alkaline formation waters and hydrothermal fluids. During their upwelling, hydrothermal fluids carried large amounts of Ca^{2+} into the Eocene Shahejie Formation, increasing the calcium saturation in the primary alkaline formation waters.

The carbon isotope compositions of carbonate cements provide important insights into the origin and nature of the carbon sources involved during diagenesis. The low $\delta^{13}C$ values (V-PDB) in carbonate cements can result from several mechanisms: (1) input of marine dissolved inorganic carbon (e.g. Walter et al., 2007; Savard et al., 2021); (2) contributions from deep-sourced magmatic CO_2 associated with hydrothermal activity (e.g. Parks et al., 2013; Cinti et al., 2017). (3) infiltration of atmospheric CO_2 via meteoric water interaction (e.g. Morad, 1998; Yuan et al., 2017); (4) soil CO_2 derived from soil respiration (e.g. Cerling, 1984; Da et al., 2020); and (5) thermal degradation of organic matter in sediments (e.g. Nelson and Lawrence, 1984; Wang et al., 2016). In the present study, carbonate cements were precipitated under non-marine conditions, effectively ruling out contributions from marine dissolved inorganic carbon (DIC). Based on carbon isotopic evidence, most $\delta^{13}C$ values of the carbonate cements fall within the range typically associated with magmatic CO_2 and air CO_2 (Fig. 11). Regarding the magmatic CO_2. During the ascent and cooling of magma from the crust or upper mantle, substantial amounts of volatile substances, such as CO_2, are released. These CO_2 typically exist in dissolved form, with some remaining in a gaseous state. Both forms migrate upward with the hydrothermal fluids, ultimately reaching the surface or shallower strata (Tingle and Green, 1987). Once the CO_2 enters the target formation, it rapidly combines with Ca^{2+}, resulting in the 'instantaneous' precipitation of substantial amounts of calcite cement within the pore spaces. And the carbonate cements in the study area exhibit markedly depleted $\delta^{18}O$ values, ranging from −14.0 ‰ to −11.1 ‰. According to Śliwiński et al. (2016), such strongly negative $\delta^{18}O$ signatures reflect elevated temperatures during diagenesis, which is consistent with the interpretation of hydrothermal activity in the region. With regard to air CO_2, the carbonate cements in the study area were formed during the synsedimentary to early diagenetic stages, when sediments were subjected to subaerial exposure or influenced by shallow meteoric water infiltration. Air CO_2 could have been introduced into the subsurface along with meteoric water percolation, increasing the concentration of dissolved

inorganic carbon in pore waters and thereby promoting carbonate precipitation. In addition, only one $\delta^{13}C$ value of the carbonate cements falls within the typical range of soil-derived CO_2, suggesting that soil systems at or near the surface may have influenced the shallow burial environment, albeit to a limited extent. Overall, the carbon incorporated into the carbonate cements is interpreted to be a mixture of magmatic and air CO_2, with a potential but limited contribution from soil CO_2. Among these sources, magmatic CO_2, owing to its high flux rate, is considered the dominant contributor, reflecting the critical role of deep hydrothermal activity in driving the diagenetic cementation process.

In summary, the formation process of carbonate cements in the Eocene Shahejie Formation sandstones of the Dongying Depression can be outlined as follows: During the synsedimentary to early diagenetic stages of the Eocene Shahejie Formation sandstones (39.4 ± 1.9 Ma for Sample Z20-7 and 42 ± 7.6 Ma for Sample T36-2), the sediments experienced limited compaction, with particles primarily exhibiting point contact or minimal interaction. During this stage, air CO_2 infiltrated the subsurface via meteoric precipitation, while the surficial soil system contributed additional soil CO_2 to the pore waters, collectively enhancing the concentration of inorganic carbon in the primary saline water. Under the influence of New Pacific Plate subduction, magmatic activity and associated hydrothermal fluid activity in the Dongying Depression were frequent. Deep hydrothermal fluids upwelled along extensional large faults (e.g., the Gaoqing-Pingnan Fault), leading to the release of substantial magmatic CO_2 from the degassing of these fluids. Acting as key transport agents, the hydrothermal fluids carried both magmatic CO_2 and deep metal ions into the target layers, resulting in supersaturation of calcium carbonate in the saline formation waters, which caused the 'instantaneous' precipitation of calcite cement between particles. Ultimately, blocky carbonate cement formed in the low-matrix sandstones, while scattered patchy calcite appeared in the high-matrix sandstones. Sandstones farther from the fault zones, less affected by hydrothermal fluid circulation, exhibited no significant carbonate cementation (Fig. 13).

5.4. Carbonate cement formation mode

The diagenetic evolution of the sandstone in the Eocene Shahejie Formation, Dongying Depression, can be divided into three stages.

1 *Pre-hydrothermal influence stage* (50–40 Ma). During the deposition of the Eocene Shahejie Formation, Dongying Depression was primarily characterized by the development of deltaic and shallow lacustrine sand bodies, which resulted in interbedding of matrix-rich sandstones with matrix-poor sandstones (Fig. 8). During this stage, the Eocene Shahejie Formation was in early burial and had not yet undergone significant compaction. Grain contacts were predominantly non-contact to point-contact. Compared to matrix-rich sandstones (Fig. 14A1), matrix-poor sandstones exhibited superior initial petrophysical properties (Fig. 14B1).

2 *Hydrothermal intensive influence stage* (~40 Ma). Prior to significant compaction, the study area underwent intense hydrothermal activity, with hydrothermal fluids percolating into the target strata along basement faults (Jin et al., 2004; Liang et al., 2024), inducing a rapid increase in formation temperature. Simultaneously, the influx of large amounts of Ca^{2+} and CO_2 led to the supersaturation of diagenetic fluids with calcium carbonate, resulting in the precipitation of substantial quantities of carbonate cements within the pores. In particular, matrix-poor sandstones were profoundly influenced by hydrothermal activity, leading to the formation of blocky calcite cement between the grains, which almost entirely filled the pore spaces (Fig. 14B2). In contrast, matrix-rich sandstones, which exhibit relatively inferior initial petrophysical properties, experienced a more limited influence from hydrothermal fluids due to their poor permeability. As a result, only a modest quantity of scattered patchy calcite was formed between the grains, occupying a fraction of the original pore space (Fig. 14A2). However, sandstones that remained unaffected by hydrothermal fluids showed negligible carbonate cementation (Fig. 14C2).

3 *Post-hydrothermal influence stage* (<40 Ma). During this stage, due to relatively rapid subsidence, the Eocene Shahejie Formation in the study area underwent intense compaction. Matrix-poor sandstones,

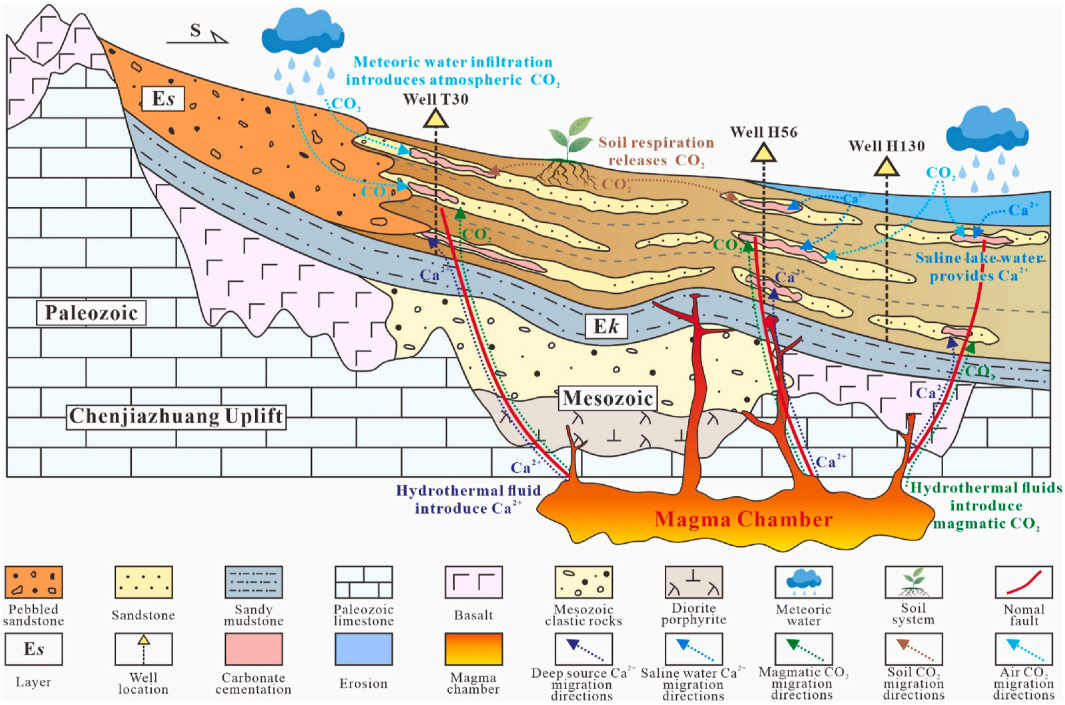

Fig. 13. The source model of carbonate cement in the Eocene Shahejie Formation, Dongying Depression.

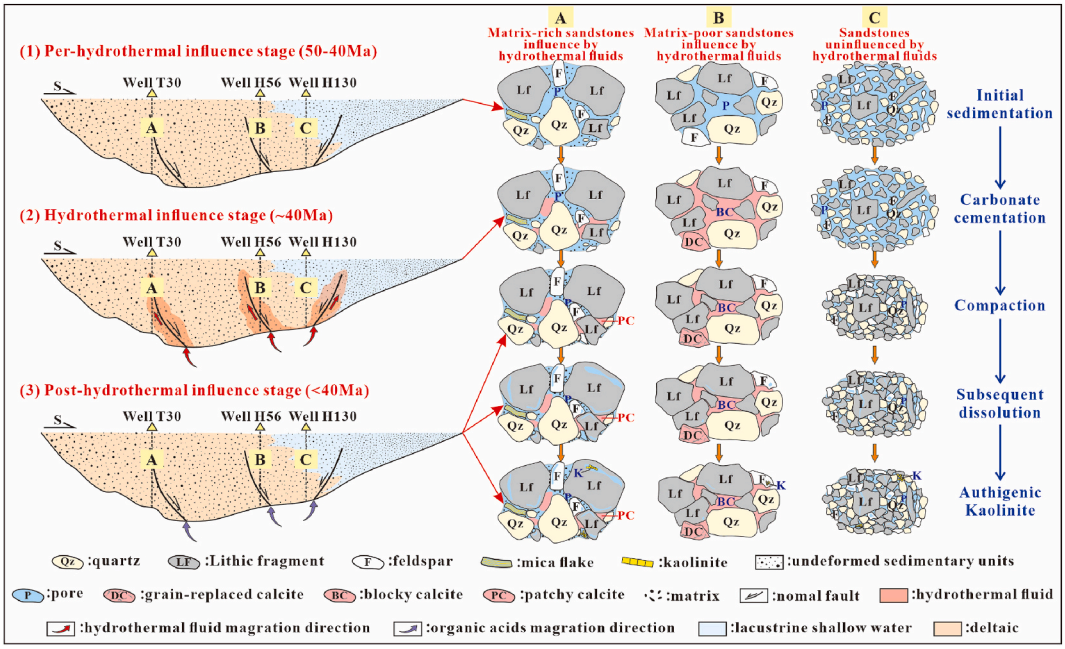

Fig. 14. Diagenetic evolution model under hydrothermal influence in the Eocene Shahejie Formation, Dongying Depression.

influenced by hydrothermal fluids, contained blocky carbonate cement, which effectively resisted strong compaction. The grains in these matrix-poor sandstones remained unconnected and were 'floating' within the cement. However, the presence of carbonate cement significantly reduced the permeability of the sandstone, impeding organic acid infiltration and resulting in limited subsequent dissolution (Fig. 14B3). In contrast, matrix-rich sandstones with scattered patchy calcite (Fig. 14A3), as well as sandstones unaffected by hydrothermal fluids, which contained minimal carbonate cement (Fig. 14C3), were unable to resist intense burial compaction. This led to significant plastic deformation of mica flakes and lithic fragments, causing a marked reduction in intergranular porosity. However, under the influence of organic acids during later diagenesis, both sandstone types experienced differential dissolution, resulting in intergranular and intragranular dissolution pores. Although some of these pores were later filled with kaolinite, the petrophysical properties of the matrix-rich sandstones and hydrothermally unaffected sandstones remained superior to those of the matrix-poor sandstones.

6. Conclusion

The results of this integrated study provide strong evidence supporting the material origin and formation timing of the hydrothermally derived carbonate cements in the sandstones of the Eocene Shahejie Formation, Dongying Depression.

Extensive carbonate cementation is observed in the sandstones near the faults of the Eocene Shahejie Formation, Dongying Depression. Petrographic and EPMA analyses indicate that calcite is the primary component of these carbonate cements, forming during the early diagenetic stage. The morphology of calcite differs depending on sandstone maturity. Matrix-poor sandstones commonly exhibit blocky calcite cement, while matrix-rich sandstones primarily contain scattered patchy calcite. Fluid inclusion analyses indicate homogenization temperatures of 85–350 °C, suggesting calcite formation under elevated thermal conditions. The carbonate cements exhibit low $\delta^{13}C$ (−11.8 to −3.1 ‰ VPDB) and $\delta^{18}O$ (clustered tightly from −14.0 to −11.1 ‰ VPDB) values, which suggest that the carbon was derived from a mixed source comprising magmatic CO_2, air CO_2, and a potential contribution from soil CO_2.

Under the influence of Cenozoic New Pacific Plate subduction, volcanic and hydrothermal activities were exceptionally frequent in Dongying Depression. Ca^{2+} and CO_2 were introduced into the Eocene Shahejie Formation via hydrothermal fluids, leading to the supersaturation of calcium carbonate in the alkaline formation water and then 'instantaneously' precipitation of substantial amounts of calcite cements. This study utilized *in situ* U-Pb isotopic dating of calcite to constrain the timing of hydrothermal activity to between 39.4 ± 1.9 Ma and 42 ± 7.6 Ma.

This study is among the few to integrate *in situ* U-Pb isotopic dating of calcite in combination with other advanced techniques for analyzing intergranular carbonate cements in clastic rocks. It establishes a novel framework for constraining the material origin and precipitation timing of carbonate cements, thereby demonstrating the broad applicability of *in situ* U-Pb isotopic dating of calcite in the field of clastic rock studies. Additionally, the timing of hydrothermal activity in the Shahejie Formation determined in this study offers crucial constraints on tectonic-magmatic activity in the Dongying Depression.

CRediT authorship contribution statement

Yishan Gao: Writing – original draft. **Shifa Zhu:** Writing – review & editing, Resources. **Hang Cui:** Writing – review & editing. **Wendian Cai:** Investigation. **Ruihang Zhang:** Investigation.

Declaration of competing interest

The authors declare that they have no known competing financial interests or personal relationships that could have appeared to influence the work reported in this paper.

Acknowledgements

This work was supported by the National Natural Science Foundation of China (42272109). We thank Sinopec Shengli Oilfield Company for permission to use industry data for this research. Thanks to the Associate Editor, Lin Ma for valuable comments and suggestions, which helped us to significantly improve the manuscript. We also would like to thank two

anonymous reviewers for valuable comments and constructive modifications that greatly enhanced the manuscript. Finally, we thank Professor Jing Sun and Dr Wenxia Yang for their help with the experimental operation of carbonate U-Pb geochronology in this paper.

Appendix A. Supplementary data

Supplementary data to this article can be found online at https://doi.org/10.1016/j.marpetgeo.2025.107513.

Data availability

Data will be made available on request.

References

Barbieri, M., Boschetti, T., Barberio, M.D., Billi, A., Franchini, S., Iacumin, P., Selmo, E., Petitta, M., 2020. Tracing deep fluid source contribution to groundwater in an active seismic area (Central Italy): a combined geothermometric and isotopic ($\delta^{13}C$) perspective. J. Hydrol. 582, 124495.

Carvalho, M.V.F., De Ros, L.F., Gomes, N.S., 1995. Carbonate cementation patterns and diagenetic reservoir facies in the Campos Basin Cretaceous turbidites, offshore eastern Brazil. Mar. Petrol. Geol. 12 (7), 741–758.

Cerling, T.E., 1984. The stable isotopic composition of modern soil carbonate and its relationship to climate. Earth Planet Sci. Lett. 71 (2), 229–240.

Chang, J., Qiu, N., Zhao, X., Shen, F., Liu, N., Xu, W., 2018. Mesozoic and Cenozoic tectono-thermal reconstruction of the western Bohai Bay Basin (East China) with implications for hydrocarbon generation and migration. J. Asian Earth Sci. 160, 380–395.

Chen, Z., Qiao, R., Li, C., Wang, D., Gao, Y., 2022. Hydrocarbon generation potential and model of the deep lacustrine source rocks in the Dongying Depression, Bohai Bay Basin. Mar. Petrol. Geol. 140, 105656.

Cinti, D., Tassi, F., Procesi, M., Brusca, L., Cabassi, J., Capecchiacci, F., Huertas, A.D., Galli, G., Grassa, F., Vaselli, O., Voltattorni, N., 2017. Geochemistry of hydrothermal fluids from the eastern sector of the Sabatini Volcanic District (central Italy). Appl. Geochem. 84, 187–201.

Cui, H., Zhu, S., Tan, M., Tong, H., 2022. Depositional and diagenetic processes in volcanic matrix-rich sandstones from the Shanxi and Shihezi formations, Ordos Basin, China: implication for volcano-sedimentary systems. Basin Res. 34 (6), 1859–1893.

Cui, H., Zhu, S., Liang, C., Ma, W., Tong, H., Shi, Z., 2023. Facies association analysis of a Toarcian siliciclastic-carbonate lacustrine system, Sichuan Basin, China. Palaeogeography. Palaeoclimatology, Palaeoecology. 631, 111841.

Cui, H., Zhu, S., Gao, Y., Chen, W., 2024. Hydrothermal activity near the Permian–Triassic transition in the south-western Ordos Basin, China: evidence from carbonate cementation in Upper Permian sandstones. Sedimentology 72 (1), 227–257.

Da, J., Zhang, Y.G., Li, G., Ji, J., 2020. Aridity-driven decoupling of $\delta^{13}C$ between pedogenic carbonate and soil organic matter. Geology 48 (10), 981–985.

Davies, G.R., Smith Jr, L.B., 2006. Structurally controlled hydrothermal dolomite reservoir facies: an overview. AAPG Bull. 90 (11), 1641–1690.

De Boever, E., Brasier, A.T., Foubert, A., Kele, S., 2017. What do we really know about early diagenesis of nonmarine carbonates? Sed. Geol. 361, 25–51.

Dou, L., Hou, J., Liu, Y., Zhang, L., Song, S., Wang, X., 2020. Sedimentary infill of shallow water deltaic sand bodies controlled by small-scale syndepositional faults related paleogeomorphology: insights from the paleogene Shahejie formation in the Dongying depression, Bohai Bay Basin, Eastern China. Mar. Petrol. Geol. 118, 104420.

Dutton, S.P., 2008. Calcite cement in Permian deep-water sandstones, Delaware Basin, west Texas: origin, distribution, and effect on reservoir properties. AAPG Bull. 92 (6), 765–787.

Feng, Y., Li, S., Lu, Y., 2013. Sequence stratigraphy and architectural variability in late Eocene lacustrine strata of the Dongying Depression, Bohai Bay Basin, eastern China. Sediment. Geol. 295, 1–26.

Folk, R.L., 1974. Petrology of Sedimentary Rocks. Hemphill publishing company.

Goldstein, R., Reynolds, J., 1994. Systematics of fluid inclusions. SEPM short course notes 31, 188.

Hein, J.R., Zierenberg, R.A., Maynard, J.B., Hannington, M.D., 2007. Barite-forming environments along a rifted continental margin, Southern California Borderland. Deep Sea Res. Part II Top. Stud. Oceanogr. 54 (11–13), 1327–1349.

Hill, C.A., Polyak, V.J., Asmerom, Y., Provencio, P.P., 2016. Constraints on a Late Cretaceous uplift, denudation, and incision of the Grand Canyon region, southwestern Colorado Plateau, USA, from U-Pb dating of lacustrine limestone. Tectonics 35 (4), 896–906.

Hou, Z., Chen, S., Liu, H., Yang, H., Li, H., Wang, Y., 2019. Hydrothermal fluid activity and its hydrocarbon geological significance in Dongying Depression. J. China Inst. Min. Technol. 48 (5), 1090–1101 (in Chinese with English abstract).

Hu, S., O'Sullivan, P.B., Raza, A., Kohn, B.P., 2001. Thermal history and tectonic subsidence of the Bohai Basin, northern China: a Cenozoic rifted and local pull-apart basin. Phys. Earth Planet. Inter. 126 (3–4), 221–235.

Jin, C., Qiao, D., Dan, W., 2012. Meso-Cenozoic volcanic rock distribution and reservoir characteristics in the Bohai Bay Basin. Oil Gas Geol. 33 (1), 19–29 (in Chinese with English abstract).

Jin, X., Zhao, J., Feng, Y., Hofstra, A.H., Deng, X., Zhao, X., Li, J., 2021. Calcite U-Pb dating unravels the age and hydrothermal history of the giant Shuiyindong Carlin-type gold deposit in the golden triangle, South China. Econ. Geol. 116 (6), 1253–1265.

Jin, Z., Zhang, L., Yang, L., Hu, W., 2004. A preliminary study of mantle-derived fluids and their effects on oil/gas generation in sedimentary basins. J. Petrol. Sci. Eng. 41 (1–3), 45–55.

Lafay, R., Baumgartner, L.P., Stephane, S., Suzanne, P., German, M.H., Torsten, V., 2017. Petrologic and stable isotopic studies of a fossil hydrothermal system in ultramafic environment (Chenaillet ophicalcites, Western Alps, France): processes of carbonate cementation. Lithos 294, 319–338.

Lampe, C., Song, G., Cong, L., Mu, X., 2012. Fault control on hydrocarbon migration and accumulation in the Tertiary Dongying depression, Bohai Basin, China. AAPG Bull. 96 (6), 983–1000.

Lao, H., Shan, Y., Wang, Y., Wu, Z., 2020. Characteristics of growth fault architecture and its evolution in mudstone strata: evidence from the core of Bohai Bay basin. Mar. Petrol. Geol. 119, 104503.

Li, C., Zeng, J., Liu, S., Dong, Y., Wang, M., 2024a. How did submarine volcanic eruptions interact with organic matter to favour hydrocarbon generation in the Bohai Bay Basin, China. Int. Geol. Rev. 66 (13), 2345–2364.

Li, F., Li, W., 2016. Controlling factors for dawsonite diagenesis: a case study of the Binnan Region in Dongying Sag, Bohai Bay Basin, China. Aust. J. Earth Sci. 63 (2), 217–233.

Li, F., Li, W., 2017. Petrological record of CO_2 influx in the Dongying sag, Bohai Bay Basin, NE China. Appl. Geochem. 84, 373–386.

Li, H., Huang, X., Guo, H., 2014. Geochemistry of Cenozoic basalts from the Bohai Bay Basin: implications for a heterogeneous mantle source and lithospheric evolution beneath the eastern North China Craton. Lithos 196, 54–66.

Li, W., Wu, X., Li, Y., Zhang, Y., Zhang, X., Wang, H., 2024b. Igneous intrusion contact metamorphic system and its reservoir characteristics: a case study of Paleogene Shahejie Formation in Nanpu sag of Bohai Bay Basin, China. Petrol. Explor. Dev. 51 (2), 320–336.

Li, Y., Fan, A., Yang, R., Lash, G., Bilal, A., Chen, J., 2022. A multi-faceted approach to determine the provenance of Eocene converging deltas, Dongying Depression, Bohai Bay Basin (E China). Mar. Petrol. Geol. 141, 105692.

Li, Z., Rankenburg, K., Normore, L.S., Evans, N.J., Mclnnes, B.I.A., Dent, L.M., Fielding, I. O.H., 2023. *In situ* calcite U-Pb geochronology of carbonate and clastic sedimentary rocks from the Canning Basin, Western Australia. Aust. J. Earth Sci. 70 (3), 332–343.

Liang, J., Wang, H., Bai, Y., Ji, X., Dou, X., 2016. Cenozoic tectonic evolution of the Bohai Bay Basin and its coupling relationship with Pacific Plate subduction. J. Asian Earth Sci. 127, 257–266.

Liang, T., Jiao, M., Ma, X., Zhang, L., 2024. Impacts of mantle-derived fluids on source-related biomarkers in crude oils: a case study from the Dongying Depression, eastern China. Pet. Sci. 21 (6), 3706–3719.

Liu, J., Xian, B., Wang, J., Ji, Y., Lu, Z., Liu, S., 2017. Sedimentary architecture of a sub-lacustrine debris fan: Eocene Dongying Depression, Bohai Bay Basin, east China. Sediment. Geol. 362, 66–82.

Liu, K., Zhang, J., Xiao, W., Wilde, S.A., Alexandrov, I., 2020. A review of magmatism and deformation history along the NE Asian margin from ca. 95 to 30 ma: transition from the Izanagi to Pacific plate subduction in the early Cenozoic. Earth Sci. Rev. 209, 103317.

Luo, J., Li, C., Lei, C., Cao, J., Song, K., 2020. Discussion on research advances and hot issues in diagenesis of clastic-rock reservoirs. Journal of Palaeography 22 (6), 1021–1040 (in Chinese with English abstract).

Ma, B., Eriksson, K.A., Cao, Y., Jia, Y., Wang, Y., Gill, B.C., 2016. Fluid flow and related diagenetic processes in a rift basin: evidence from the fourth member of the Eocene Shahejie Formation interval, dongying depression, Bohai Bay Basin, China. AAPG Bull. 100, 1633–1662.

Machel, l.H.G., Lonnee, J., 2002. Hydrothermal dolomite—A product of poor definition and imagination. Sediment. Geol. 152 (3–4), 163–171.

Menezes, C.P., Bezerra, F.H.R., Balsamo, F., Mozafari, M., Vieira, M.M., Srivastava, N.K., de Castro, D.L., 2019. Hydrothermal silicification along faults affecting carbonate-sandstone units and its impact on reservoir quality, Potiguar Basin, Brazil. Mar. Petrol. Geol. 110, 198–217.

Meng, J., Jiang, Z., Yang, Y., Nian, T., 2021. Soft-sediment deformation structures in a lacustrine depositional context: an example from the Eocene Dongying Depression in the Bohai Bay Basin, East China. Sediment. Geol. 426, 106039.

Mills, R.A., Elderfield, H., 1995. Hydrothermal activity and the geochemistry of metalliferous sediment. Seafloor hydrothermal systems: physical, chemical, biological, and geological interactions 91, 392–407.

Morad, S., 1998. Carbonate cementation in sandstones: distribution patterns and geochemical. In: Morad, S. (Ed.), Carbonate Cementation in Sandstones, vol. 26. Special Publication International Association of Sedimentologists.

Morad, S., Al-Ramadan, K., Ketzer, J.M., De Ros, L.F., 2010. The impact of diagenesis on the heterogeneity of sandstone reservoirs: a review of the role of depositional facies and sequence stratigraphy. AAPG Bull. 94 (8), 1267–1309.

Nelson, C.S., Lawrence, M.F., 1984. Methane-derived high-Mg calcite submarine cement in Holocene nodules from the Fraser Delta, British Columbia, Canada. Sedimentology 31 (5), 645–654.

Nuriel, P., Craddock, J., Kylander-Clark, A.R.C., Uysal, I.T., Karabacak, V., Dirik, R.K., Hacker, B.R., Weinberger, R., 2019. Reactivation history of the North Anatolian fault zone based on calcite age-strain analyses. Geology 47 (5), 465–469.

Parks, M.M., Caliro, S., Chiodini, G., Pyle, D.M., Mather, T.A., Berlo, K., Edmonds, M., Biggs, J., Nomikou, P., Raptakis, C., 2013. Distinguishing contributions to diffuse CO_2 emissions in volcanic areas from magmatic degassing and thermal decarbonation using soil gas ^{222}Rn-$\delta^{13}C$ systematics: Application to Santorini aolcano, Greece. Earth Planet Sci. Lett. 377, 180–190.

Roberts, N.M.W., Drost, K., Horstwood, M.S.A., Condon, D.J., Chew, D., Drake, H., Milodowski, A.E., McLean, N.M., Smye, A.J., Walker, R.J., Haslam, R., Hodson, K., Imber, J., Beaudoin, N., Lee, J.K., 2020. Laser ablation inductively coupled plasma mass spectrometry (LA-ICP-MS) U-Pb carbonate geochronology: strategies, progress, and limitations. Geochronology 2 (1), 33–61.

Roberts, N.M.W., Walker, R.J., 2016. U-Pb geochronology of calcite-mineralized faults: absolute timing of rift-related fault events on the northeast Atlantic margin. Geology 44 (7), 531–534.

Savard, M.M., Jautzy, J.J., Lavoie, D., Dhillon, R.S., Defliese, W.F., 2021. Clumped and oxygen isotopes reveal differential disequilibrium in the formation of carbonates from marine methane seeps. Geochem. Cosmochim. Acta 298, 43–54.

Śliwiński, M.G., Kozdon, R., Kitajima, K., Denny, A., Valley, J.W., 2016. Microanalysis of carbonate cement $\delta^{18}O$ in a CO_2-storage system seal: Insights iito the diagenetic history of the Eau Claire Formation (Upper Cambrian), Illinois Basin. AAPG (Am. Assoc. Pet. Geol.) Bull. 100 (6), 1003–1031.

Smith, Jr.L.B., Davies, G.R., 2006. Structurally controlled hydrothermal alteration of carbonate reservoirs: introduction. AAPG (Am. Assoc. Pet. Geol.) Bull. 90 (11), 1635–1640.

Su, A., Chen, H., Feng, Y., Zhao, J., Wang, Z., Hu, M., Jiang, H., Nguyen, A.D., 2022. *In situ* U-Pb dating and geochemical characterization of multi-stage dolomite cementation in the Ediacaran Dengying Formation, Central Sichuan Basin, China: constraints on diagenetic, hydrothermal and paleo-oil filling events. Precambr. Res. 368, 106481.

Tingle, N.T., Green, H.W., 1987. Carbon solubility in olivine: implications for upper-mantle evolution. Geology 15, 324–326.

Urabe, T., Kusakabe, M., 1990. Barite silica chimneys from the Sumisu Rift, Izu-Bonin Arc: possible analog to hematitic chert associated with Kuroko deposits. Earth Planet Sci. Lett. 100 (1–3), 283–290.

Walter, L.M., Ku, T.C.W., Muehlenbachs, K., Patterson, W.P., Bonnell, L., 2007. Controls on the $\delta^{13}C$ of dissolved inorganic carbon in marine pore waters: An integraaed case study of isotope exchange during syndepositional recrystallization of biogenic carbonate sediments (South Florida Platform, USA). Deep Sea Res. Part II Top. Stud. Oceanogr. 54 (11–13), 1163–1200.

Wang, G., Li, S., Suo, Y., Zhang, X., Zhang, Z., Wang, D., Liu, Z., Liu, Y., Zhou, J., Wang, P., Guo, L., 2022. Deep-shallow coupling response of the Cenozoic Bohai Bay Basin to plate interactions around the Eurasian Plate. Gondwana Res. 102, 180–199.

Wang, J., Cao, Y., Liu, K., Xue, X., Xu, Q., 2016. Pore fluid evolution, distribution and water-rock interactions of carbonate cements in red-bed sandstone reservoirs in the Dongying Depression, China. Mar. Petrol. Geol. 72, 279–294.

Wang, L., Han, Y., Lou, D., He, Z., Guo, X., Steele-MacInnis, M., 2024. Hydrothermal petroleum related to intracontinental magmatism in the Bohai Bay Basin, eastern China. Mar. Petrol. Geol. 167, 106982.

Worden, R.H., Matray, J.M., 1998. Carbonate cement in the Triassic Chaunoy Formation of the Paris Basin: distribution and effect on flow properties. Carbonate Cementation in Sandstones: Distribution Patterns and Geochemical Evolution, pp. 163–177.

Worden, R.H., Burley, S.D., 2003. Sandstone diagenesis: the evolution of sand to stone. Sandstone Diagenesis: Recent and Ancient, pp. 1–44.

Wu, C., Gu, L., Zhang, Z., Ren, Z., Chen, Z., Li, W., 2006. Formation mechanisms of hydrocarbon reservoirs associated with volcanic and subvolcanic intrusive rocks: examples in Mesozoic–Cenozoic basins of eastern China. AAPG Bull. 90 (1), 137–147.

Wu, J., Liang, C., Yang, R., Xie, J., 2022. Sequence stratigraphic control on the variations of organic matter in Eocene lacustrine shales within the Dongying Depression, eastern China. J. Asian Earth Sci. 237, 105353.

Wu, J.T.J., Wu, J., 2019. Izanagi-Pacific ridge subduction revealed by a 56 to 46 Ma magmatic gap along the northeast Asian margin. Geology 47 (10), 953–957.

Wu, Y., Wang, J., Duan, D., Zhao, J., Zhang, C., Mao, J., Xiong, S., Jiang, S., 2024. Linking carbonate-hosted Zn-Pb deposit to deep mantle activity: evidence from *in situ* U-Pb geochronology of calcite from the world-class Huayuan Zn-Pb ore field in South China. Chem. Geol. 643, 121823.

Xi, K., Cao, Y., Liu, K., Wu, S., Yuan, G., Zhu, R., Zhao, Y., Hellevang, H., 2019. Geochemical constraints on the origins of calcite cements and their impacts on reservoir heterogeneities: a case study on tight oil sandstones of the Upper Triassic Yanchang Formation, southwestern Ordos Basin, China. AAPG (Am. Assoc. Pet. Geol.) Bull. 103 (10), 2447–2485.

Xu, X., Zuza, A.V., Chen, L., Zhu, W., Yin, A., Fu, X., Gao, S., Xu, X., Kuang, X., Zhang, F., Lei, W., Lin, X., Chen, H., Yang, S., 2021. Late cretaceous to early Cenozoic extension in the Lower Yangtze region (East China) driven by Izanagi-Pacific plate subduction. Earth Sci. Rev. 221, 103790.

Yan, Z., Ji, H., Guo, G., Xia, F., Zhang, W., Song, S., Liu, S., 2023. Geochemical characteristics of trace elements and REEs and their geological significance for uranium mineralization within the qianjiadian sandstone-hosted uranium deposit, songliao Basin. Geofluids 2023 (1), 6297033.

Yang, P., Liu, K., Li, Z., Rankenburg, K., McInnes, B.I.A., Liu, J., Evans, N.J., 2022. Direct dating Paleo-fluid flow events in sedimentary basins. Chem. Geol. 588, 120642.

Yang, T., Cao, Y., Friis, H., Liu, K., Wang, Y., Zhou, L., Zhang, S., Zhang, H., 2018. Genesis and distribution pattern of carbonate cements in lacustrine deep-water gravity-flow sandstone reservoirs in the third member of the Shahejie Formation in the Dongying Sag, Jiyang Depression, Eastern China. Mar. Petrol. Geol. 92, 547–564.

Yang, Y., Kra, K.L., Qiu, L., Yang, B., Dong, D., Wang, Y., Khan, D., 2023. Impact of sedimentation and diagenesis on deeply buried sandy conglomerate reservoirs quality in nearshore sublacustrine fan: a case study of lower Member of the Eocene Shahejie Formation in Dongying Sag, Bohai Bay Basin (East China). Sediment. Geol. 444, 106317.

Yuan, G., Cao, Y., Zhang, Y., Gluyas, J., 2017. Diagenesis and reservoir quality of sandstones with ancient “deep” incursion of meteoric freshwater-an example in the Nanpu Sag, Bohai Bay Basin, East China. Mar. Petrol. Geol. 82, 444–464.

Zahid, M.A., Dong, C., Lin, C., Gluyas, J., Jones, S., Zhang, X., Munawar, M.J., Ma, C., 2016. Sequence stratigraphy, sedimentary facies and reservoir quality of Es4s, southern slope of Dongying Depression, Bohai Bay Basin, East China. Mar. Petrol. Geol. 77, 448–470.

Zeng, J., Jin, Z., Zhang, L., 2004. Mantle-derived fluids flow along the Gaoqing-Pingnan fault and its effects on oil-gas reservoir formation in the Dongying sag. Geol. Rev. 50 (5), 501–506 (in Chinese with English abstract).

Zhu, D., Liu, Q., Huang, X., Meng, Q., Wang, J., Li, P., Jin, Z., 2025. Large-scale accumulation of abiotic gases associated with subduction and volcanic activities in rift basins in eastern China. Org. Geochem. 200, 104900.

Zhu, S., Jia, Y., Cui, H., J. Dowey, P.G., Taylor, K., Zhu, X., 2019a. Alteration and burial dolomitization of fine-grained, intermediate volcaniclastic rocks under saline-alkaline conditions: Bayindulan Sag in the Er'Lian Basin, China. Mar. Petrol. Geol. 110, 621–637.

Zhu, S., Taylor, K., Chen, J., Zhu, X., Sun, S., Jia, Y., 2019b. Controls on carbonate cementation in early syn-rift terrestrial siliciclastics: the Lower Cretaceous of the Bayindulan Sag in Er'lian Basin, China. Mar. Petrol. Geol. 105, 64–80.

Zhu, Y., Liu, S., Zhang, B., Gurnis, M., Ma, P., 2021. Reconstruction of the Cenozoic deformation of the Bohai Bay basin, North China. Basin Res. 33 (1), 364–381.